



DEPARTMENT OF BIOLOGICAL AND
ENVIRONMENTAL SCIENCES

VOLATILE ORGANIC COMPOUND EMISSIONS AND SECONDARY ORGANIC AEROSOLS FORMATION DURING CLEARCUTTING OF A BOREAL FOREST AT NORUNDA, SWEDEN

Jonatan Knutsson

Degree project for Master of Science (60 hec) with a major in Environmental Science

ES2510 60 hec

Second cycle

Semester/year: Spring 2024

Supervisor: Cheng Wu, Department of Chemistry and Molecular Biology

Examiner: Mattias Hallquist, Department of Chemistry and Molecular Biology

Abstract

Emissions of biogenic volatile organic compounds (BVOCs) from boreal forest are a significant source to the global carbon emissions budget. Clearcutting, which is the most used method during forest harvesting in Sweden, can potentially lead to increased emissions of BVOC and subsequently SOA formation. In this study, we conducted observations of BVOCs oxidation products before and during an active clearcut at Norunda, Sweden, using a Filter Inlet for Gases and Aerosols (FIGAERO) coupled to a Chemical Ionization Mass Spectrometer (CIMS). We compared the oxidation products in both gas- and particle phases to their precursor VOCs. We found that during clearcutting, monoterpenes and sesquiterpenes had high temporary spikes and the averaged concentration increased by a factor of 2.8 and 3.0 respectively, while isoprene did not have spikes and averaged concentration decreased by half. The high temporary spikes in total VOCs concentration during the clearcut may have caused changes in how precursor VOCs are oxidised and that diurnal patterns changed during the clearcut. The oxidised compounds were further grouped into monoterpene-, isoprene- and sesquiterpene oxidation products based on the number of carbon atoms that they contained. All three groups showed an increased ratio during the clearcut, in both gas and particle phases, indicating an overall enhancement of their contribution to particle formation. Finally, implications that clearcutting can have on climate were discussed.

Keywords

BVOC, monoterpenes, isoprene, sesquiterpenes, clearcut, boreal forest, oxidation, mass spectrometry

Contents

1	Introduction	1
1.1	Boreal conifer forests and volatile organic compounds emissions	1
1.2	Tropospheric oxidation of VOCs	1
1.2.1	OH formation	1
1.2.2	O ₃ formation	2
1.2.3	NO ₃ formation	2
1.3	Clearcutting project	3
2	Method	4
2.1	Clearcutting at the Norunda research station	4
2.1.1	Instrument setup at field site	5
2.1.2	Instrumental description of ToF-CIMS	6
2.1.3	Instrumental description of FIGAERO	7
2.1.4	Data analysis	8
3	Results	11
3.1	Metrological conditions during the 2022 campaign	11
3.2	Effects of the clearcut on monoterpenes, isoprene and sesquiterpenes concentrations	13
3.3	Gas and particle distribution during pre-clearcut and active-clearcut period	15
3.4	Composition of gas and particle phase oxidation product	19
3.5	Impacts of the clearcutting	23
4	Discussion	29
4.1	Metrological parameters	29
4.2	The effect of clearcutting on monoterpenes, sesquiterpenes and isoprene emissions	30
4.3	Major oxidation compounds in gas and particle phases	31
4.4	Distribution of oxidation products in the gas and particle phase	32
4.5	Oxidant limitations	32
4.6	Further climate impacts	33
5	Conclusions	35
6	Appendixes	36
6.1	Table 1: Identified oxidised organic compounds	36
6.2	Arial drone images for each day of the clearcut	46
6.3	Signal variation with carbon and oxygen	47
7	References	48

1 Introduction

1.1 Boreal conifer forests and volatile organic compounds emissions

Globally boreal conifers forest covers an area of approximately 15,1 million km² and makes up 30% of all forested area. This makes it the largest biome on earth. Boreal forests emit large amounts of biogenic volatile organic compounds (BVOCs) to the atmosphere (Kivimäenpää et al., 2012). The main BVOCs emitted by boreal forest are monoterpenes, isoprene and sesquiterpenes. Emissions of BVOCs from boreal forest changes seasonally with the highest emissions during summer. As most BVOC emissions depend on temperature, and some on light, the highest emissions are seen during daytime (Vestenius et al., 2021). VOC emissions can be enhanced by mechanical wounding of conifer trees (Litvak & Monson, 1998) as these species stores high amounts of monoterpenes in their resin ducts (Ghirardo et al., 2010). A significant source of BVOC emissions could hence come from tree stems and logging residue during forest management (Haapanala et al., 2012).

Sweden is covered by large areas of forest and has historically and currently a very export-oriented forestry sector (Lindahl et al., 2017). The Swedish forest industries make up around 10% of the country's exports (Hertog et al., 2022). The forestry practice that is by far the most common in Sweden is rotation-forestry meaning that over a period of 50-100 years forest are clearcut, planted, thinned, and cut again (Ahlström et al., 2022).

1.2 Tropospheric oxidation of VOCs

Once BVOCs are emitted into the atmosphere they are oxidised either through chemical or photochemical oxidation (Goldstein & Galbally, 2007). There are three main oxidants present in the troposphere which accounts for oxidation of VOCs. These are hydroxyl radicals (OH), Ozone (O₃) and nitrate radicals (NO₃) (Finlayson-Pitts, 2000). Isoprene, monoterpenes and sesquiterpenes are unsaturated hydrocarbons causing them to react with all the mayor oxidants (OH, ozone, NO₃) (Bergström et al., 2014).

1.2.1 OH formation

OH, can be formed through several reactions in the troposphere. In remote areas OH is mainly formed through the photolysis of O₃ causing an excited O(¹D) to form which then can react with water vapour. Only a fraction of the O(¹D) that is produced in reaction 1 forms OH as in reaction 2. The remainder returns to the ground state O(³P) through reaction 2'. Since reaction 2 depends on water content in the atmosphere it becomes less important higher up in the troposphere when water content decreases with altitude (Finlayson-Pitts, 2000).



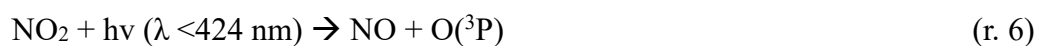
In polluted areas OH can also form from photolysis of nitrous acid (HONO) and hydrogen peroxide through reactions 3 and 4, or through reaction 5 where hydroperoxyl radical (HO₂) react with nitric oxide (NO) (Finlayson-Pitts, 2000).



Since the major formation pathways for OH is through photolysis, although there are exceptions, OH is thought to be present mainly during daytime when light can drive the reactions as described above (Finlayson-Pitts, 2000). Due to its high reactivity with other molecules and relatively high concentration (~10⁶ molecules cm³) the OH is one of the most important oxidants present in the troposphere (Seinfeld, 2016).

1.2.2 O₃ formation

O₃ is formed when NO_x (NO and NO₂) is present in sunlight. NO₂ is photolyzed to produce O(^3P) which then reacts with O₂ in the presence of a third body to produce ozone as in reactions 6 and 7 (Seinfeld, 2016).



NO₂ is then regenerated when O₃ reacts with NO (Seinfeld, 2016).



Through reactions 6,7 and 8 a steady state is formed (Seinfeld, 2016).

1.2.3 NO₃ formation

NO₃ forms when NO₂ reacts with ozone as in reaction 9. It is an important oxidant during night-time chemistry. During daytime concentrations of NO₃ are kept low as it is photolyzed and decomposes as in reaction 10 and 10'. The O(^3P) that's generated will generate O₃ from reaction with O₂ (Finlayson-Pitts, 2000).



VOCs react with the above mentioned oxidants, leading to the formation of intermediate species such as peroxy radicals (RO_2) and alkoxy radicals (RO). These intermediate species can further react with nitrogen oxides (NO_x), ozone or other radicals, leading to a variety of reaction pathways, yielding a vast amount of different oxidised products with lower volatility (Goldstein & Galbally, 2007). When low volatility oxidation products undergo gas-particle transfer, secondary organic aerosols (SOA) are formed. Aerosols affects earth's climate through effects on radiative forcing and cloud formation. Aerosols also affects human health as it has an impact on air quality. Today there is a relatively good understanding of how inorganic gases transform in the atmosphere. However, because of the vast amounts of different organic compounds present in atmosphere the knowledge of how SOA are formed is still limited (Hallquist et al., 2009).

1.3 Clearcutting project

To gain an increased understanding of how forest management effects VOC emissions and further SOA formation from boreal forests, the Norunda campaign, a joint research effort between the University of Gothenburg, Stockholm University, Lund University, ICOS and ACTRIS, has been performed from 2020 to 2023. During this campaign, the research group utilized the 2022 clearcutting event at the Norunda ACTRIS and ICOS station in the Swedish boreal forest and augmented the permanent measurements at the station with additional instruments for online and offline analysis of BVOCs, their oxidation products, and particles. These instruments were such as a VOCUS proton transfer reaction time-of-flight mass spectrometer (VOCUS-PTR-ToF-MS), a Chemical Ionization Time-of-Flight Mass Spectrometer with a Filter Inlet for Gases and Aerosols (FIGAERO-CIMS) and Neutral cluster Air Ion Spectrometer (NAIS).

This thesis focuses on the online data of BVOCs and their oxidation products before and during the clearcutting and aims to gain a better understanding of how clearcutting of boreal forests effects concentrations of VOCs, oxidation products and SOA formation. To do this, the following research questions were established.

1. What VOCs and VOC oxidation products can be found during clearcutting of boreal forests?
2. How do meteorological parameters such as wind, relative humidity, and temperature affect emissions and their oxidation?

2 Method

2.1 Clearcutting at the Norunda research station

The Norunda research station is located 30 km north of Uppsala <https://www.icos-sweden.se/norunda>. It is a boreal forest research station and was established in 1994. In 2022 the area about 300 m around the main tower at the site was turned into a clearcut (blue area in Figure 1) between July-November, including in total about 5 weeks of active clearcutting. The vegetation prior to the clearcut was mainly made up of Scots pine (*Pinus sylvestris* L.) and Norway Spruce (*Picea abies* L.) with a minor fraction of deciduous trees. The period of focus for this thesis was between the 15th of July to 2nd of August, when we had measurements with both VOCUS PTR and FIGAERO-CIMS. The pre clearcut period was between 15th – 20th of July and the active clearcutting period occurred between 24th – 29th of July. There were a few days of break without active clearcutting between 30th of July to 2nd of August. An arial drone image of the area that was clearcut between 24th to 29th is shown in Figure 2. For other arial drone images for each day of the clearcut see appendix figure S1.

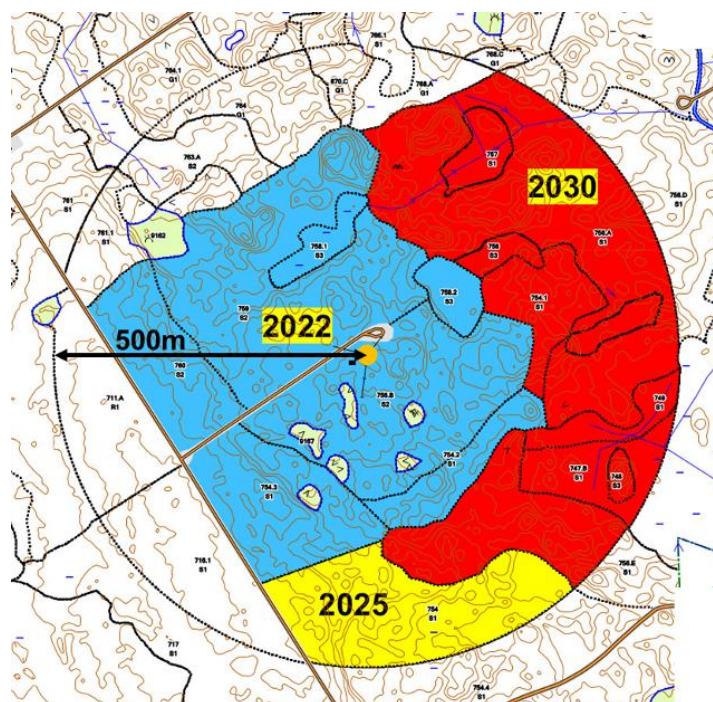


Figure 1: A map showing Areas that have been or are planned to be clearcut. Image taken from <https://www.icos-sweden.se/norunda>.



Figure 2: A map of the area that was clearcut between 24th to 29th of July 2022.

2.1.1 Instrument setup at field site

An anemometer and a sampling inlet were co-located at 35 m on the Norunda flux tower. The wind speed and direction were measured using a three-dimensional sonic anemometer (USA-1, Metek GmbH, Germany), and BVOC mixing ratios were measured using a VOCUS PTR-ToF-MS (VOCUS-2R, TOFWERK, Thun, Switzerland)(Krechmer et al., 2018). Gas- and particle-phase oxidation products were measured using a FIGAERO-CIMS (Lopez-Hilfiker et al., 2014). The flow rate through BVOC and particle inlet tubing was 20 L/min. Gases continued in a Teflon inlet into the gas port of the CIMS. Another inlet in stainless steel was used for collection of particles. The FIGAERO inlet will be described in more detail in subsequent parts. Figure 3 shows a schematic FIGAERO-CIMS and how it was setup at Norunda.

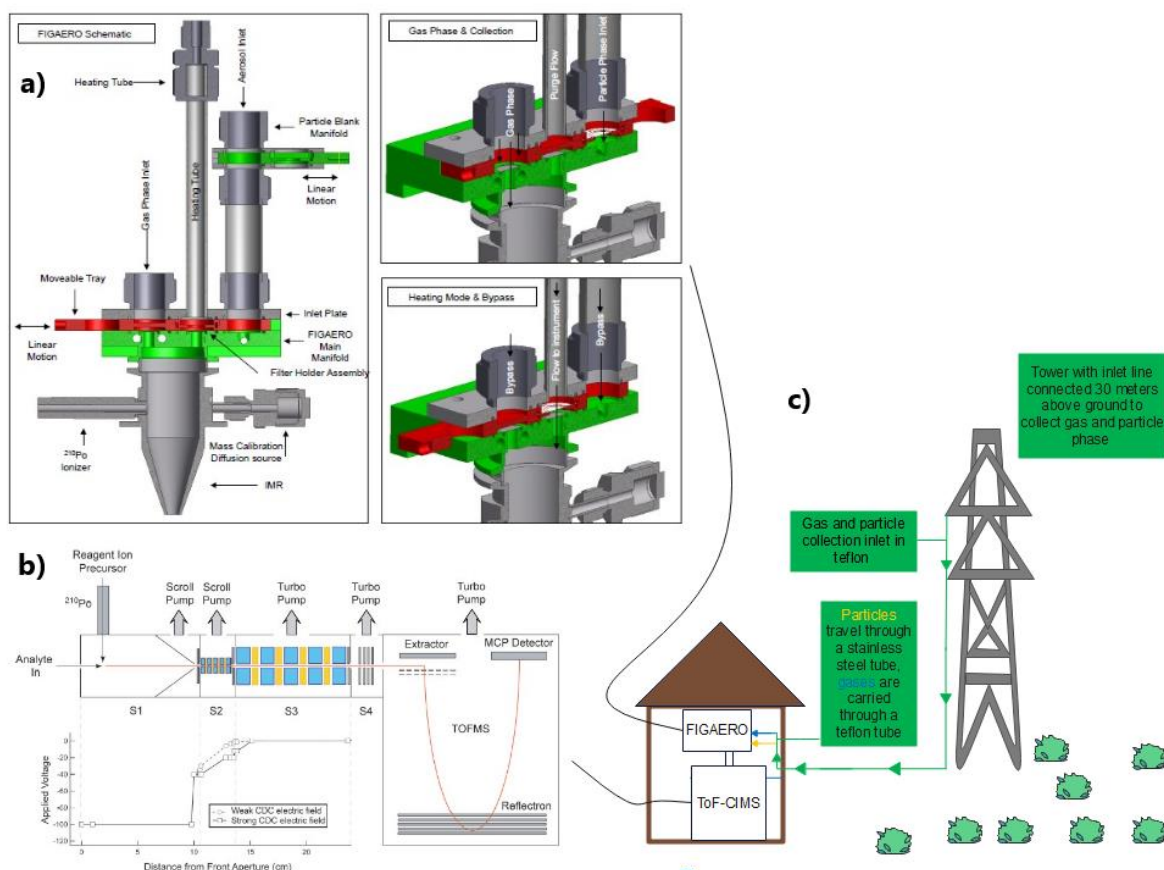


Figure 3: a) Schematic of the FIGAERO inlet, taken from Lopez et al., 2014. b) A schematic of the ToF-CIMS instrument, taken from Bertram et al., 2011. c) Schematic figure illustrating how inlet lines attached to the main tower at the Norunda station are connected to the FIGAERO-CIMS in the hut.

2.1.2 Instrumental description of ToF-CIMS.

Chemical ionization time-of-flight mass spectrometer (ToF-CIMS) is a powerful analytical tool capable of real time measurements of atmospheric trace gases. The analyte, in this case different oxidised VOCs, are introduced into an ion-molecule-reaction (IMR) chamber. In the IMR chamber ion-molecule adducts are formed (Bertram et al., 2011). The ToF-CIMS was run in iodide mode, as iodide-adduct ionization shows high sensitivity to medium and highly oxidised organic compounds (Lee et al., 2014). Ultra-High-Purity nitrogen (UHP N₂) is used as the carrier gas. The UHP N₂ flow through a permeation tube containing methyl iodide (CH₃I). The CH₃I is then carried through a Po-210 alpha emitter for ionization. I⁻ ions are generated that can form the adduct to the oxidised VOC giving it a charge (Masoud et al., 2022). Ions are introduced in a 90° angle to the flow of the analyte. The analyte, once ionised, is guided by an electric field to the ToF region of the instrument where the pressure is kept very low (1*10⁻⁶ mbar). Based on its mass to charge, different analytes are accelerated at different speeds in the

ToF region and hence reaches the detector at different times. Thus, different analytes can be separated and measured in the unit counts per second (CPS) (Bertram et al., 2011). Figure 3b show a schematic of the ToF-CIMS. A more detailed description of the CIMS instrument is provided by Bertram et al. (2011).

2.1.3 Instrumental description of FIGAERO

The design of a Filter Inlet for Gases and Aerosols (FIGAERO) allows detection of both gas and particle phase composition and can be coupled with a ToF-CIMS. To minimize cross contamination between the different phases two inlet and exit ports are used. One of the ports is used to sample and analyse gases. A second port is used for collection of particles on a polytetrafluoroethylene (PTFE) filter. When the collection of particles is done. UHP N₂ is heated and passed over the collected filter in order to vaporize the compounds to be analysed in the ToF-CIMS (Lopez-Hilfiker et al., 2014). Figure 3a show a schematic of the FIGAERO.

The sampling time for particles was 50 minutes. At the same time, the instrument was also measuring gas-phase. N₂ was added into the IMR during the first and last 2 minutes of the gas-phase sampling for gas-phase background measurement. Once gas-phase background sampling was done heating of the PTFE filter started. First the filter was heated to 200 °C over 20 minutes during the “ramp” stage. The filter was then kept at 200 °C for an additional 20 minutes during the “soak” stage. The PTFE filter was allowed to cool for 10 minutes during the cooling stage. Finally, the cycle starts again, and particles are sampled simultaneously as gas-phase is measured. For a detailed description of FIGAERO see Lopez et al (2014). Figure 4 illustrates how the FIGAERO CIMS goes through the cycles of particle phase and gas phase collection.

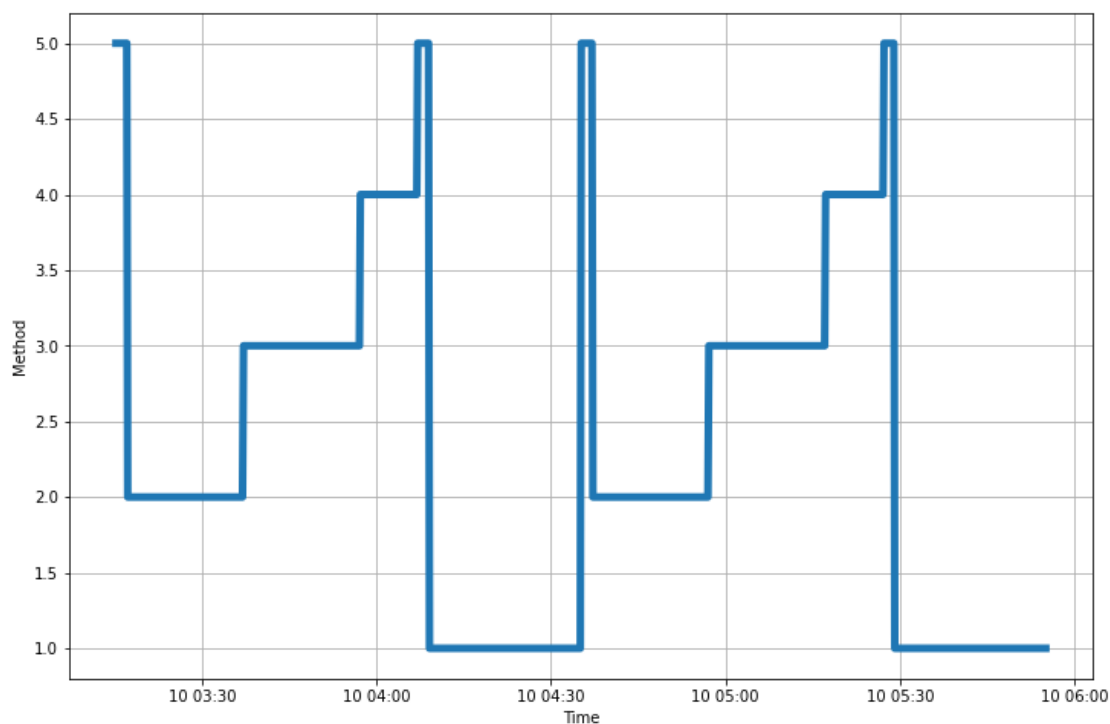


Figure 4: Plot showing how the FIGAERO-CIMS cycles through different stages. Method 1,2,3,4,5 indicates gas sampling, heating ramp, soak stage, cooling stage and background sampling respectively.

2.1.4 Data analysis

Data collected between 15th of July to 2nd of August was analysed and in total 239 cycles were analysed using Tofware v3.1.0 (Tofwerk, AG) in Igor pro v7.10 (Wavemetrics Inc) and Python. Data were first averaged to 10 second intervals. For the mass calibration, four calibrants, I^- , H_2IO^- , $C_5F_9HIO_2^-$ and $C_7F_{13}HIO_2^-$ were used to convert the ion time-of-flight to mass-to-charge (m/z) with accuracy ranging between 4 – 8 ppm. The mass resolution was approximately 3500 $m/\Delta m(\text{FWHM})$. Molecular composition was assigned to a total of 380 organic compounds.

After obtaining high resolution data from Tofware I wrote Python code for further analysis, including separating the gas and particle phase, integrating particle-phase signals, background subtraction and visualization. Signals of the each identified compounds were normalised to $(I^- + H_2IO^-) / 1000000$. Gas phase backgrounds was calculated by taking the four lowest measured datapoints during gas background sampling excluding zero values. The measured gas signal was corrected by subtracting the background signals measured within each measurement cycle. For particle phase the background signal was retrieved by first running a zero heating, meaning that a second heating was performed without collecting any particles. In total twelve of these zero heating's were done during the campaign. Thus, for correcting the particle-phase signal, I selected the particle-phase background, which was closest to the measurement. Scaling factors

were then calculated by dividing the last 3 minutes during the zero heating with the signal of the last 3 minutes during the soak stage for each FIGAERO cycle. Finally, the scaling factors were multiplied with the blanks and subtracted from particle phase signals measured during the FIGAERO cycles. Figure 5 below show an example of how background signal was removed from the particle phase. The blue datapoints is the raw signal, the red datapoints represents the scaled background and the green datapoints represents the corrected signal after background subtraction.

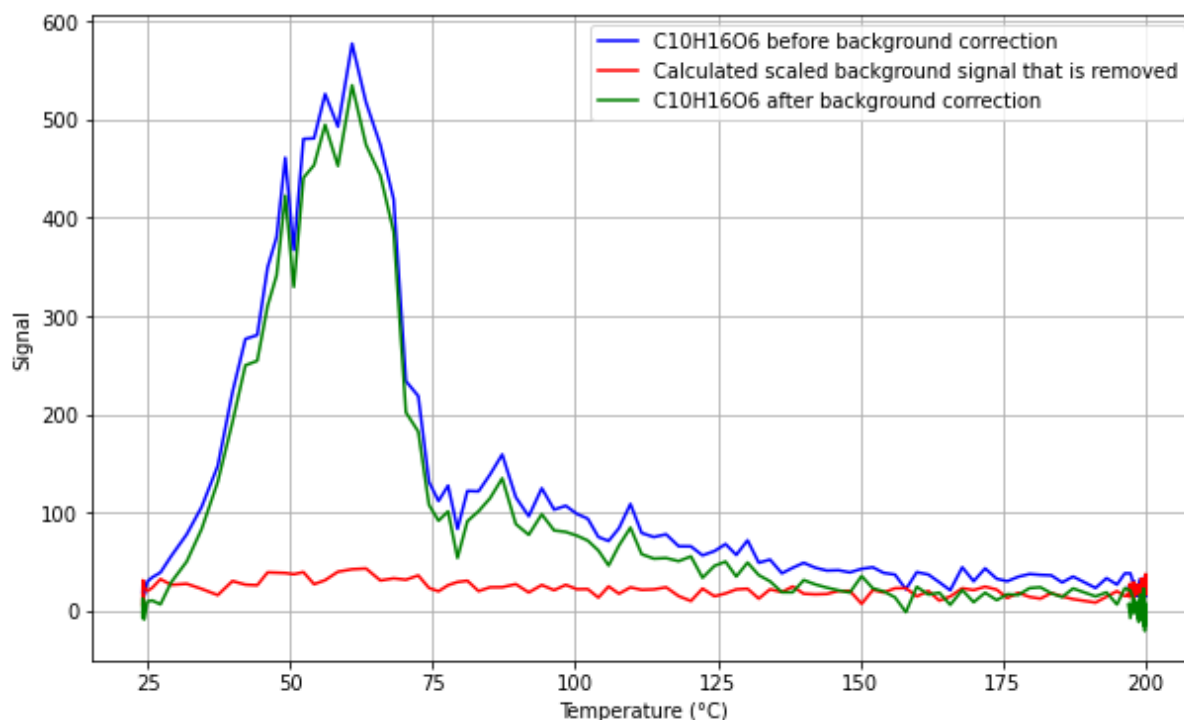


Figure 5: Example of particle-phase background correction. The blue line represents the original signal during the heating ramp. The red line is the background after applying scaling factor. The green line is the corrected signal after scaled background has been subtracted.

For gas phase, the average signals measured during the gas sampling stages were calculated. To convert the signal to concentration ($\mu\text{g}/\text{m}^3$) the following formulas were used (eq. 1 to 2).

$$gas_{conc} = \frac{gas\ signal}{g_{cal}} \quad (\text{eq. 1})$$

$$gas_{mass\ conc} = gas_{conc} * mass_{Iodide\ excluded} * p/(RT) \quad (\text{eq. 2})$$

Where p is pressure (101325 Pa), T is ambient temperature in °K, R is the universal gas law constant ($8.3143\ \text{J}\ \text{K}^{-1}\ \text{mol}^{-1}$) and g_{cal} is the calibration conversion unit (20 counts/ppt).

To get the particle phase signal for each desorption cycle, signals was firstly integrated using the trapezoidal method and then converted to the concentration (eq. 3 to 6).

$$particle_{conc} = \frac{Integrated\ particle\ signal}{(g_{cal} * Heating\ time)} \quad (eq. 3)$$

$$particle_{tot\ going\ in\ during\ heating} = particle_{conc} * \left(\frac{p}{RT}\right) * total\ flow\ to\ IMR \quad (eq. 4)$$

$$particle_{mass} = particle_{tot\ going\ in\ during\ heating} * mass_{Iodide\ excluded} \quad (eq. 5)$$

$$particle_{mass\ conc} = particle_{mass} / sample\ volume \quad (eq. 6)$$

3 Results

3.1 Metrological conditions during the 2022 campaign

The meteorological conditions will be explained in two parts. First the pre-clearcut period, 2022-07-15 to 2022-07-20 will be discussed and then the active clearcut period, 2022-07-24 to 2022-07-29 will be explained. Figure 6 shows the different meteorological parameters.

The pre-clearcut period started with two days of lower temperatures which then gradually increased throughout the pre-clearcut period. Relative humidity varied with temperature and decreased as temperature increased. There was a small amount of rain on the 15th of July, otherwise the pre-clearcut had no rain. Wind direction during the pre-clearcut period was mostly from the west and northwest. There were higher wind speeds (3-4 m/s) for the first three days of the clearcut which then decreased on the 17th and remained at around (1-2 m/s) for the rest of the pre-clearcut period. A mix of cloudy and sunny days occurred on during the pre-clearcut.

The green dotted lines in Figure 6 represents the start (at noon on the 24th of July) and the end (29th of July) of the clearcut. The active clearcut started with temperatures around 20 °C for the first two days followed by one cooler day before the temperature started to increase again. Relative humidity varied with temperature and decreased as temperature increased and vice versa as in the pre-clearcut period. There was some rain late on the 25th and during the 26th of July.

Wind direction varied throughout the active clear-cut (black dots in Figure 6b). According to the drone images Figure 6b is marked with colours to represent the extent to which it is affected by the clearcutting. Blue indicates the directions towards no-clearcutting areas, green indicate the directions towards freshly cut area (<24 hours), and yellow indicate the directions towards an area that had been clearcut on a previous day. As more and more areas around the tower were being clearcut the ranges of wind direction that would result in airmasses from the clearcut areas reaching the sample inlet increases. Overall, the air masses detected seemed to be mainly from those cut areas (both green and yellow).

Wind speeds for the active clearcut period were between 2-4 m/s for the first four days and decreased at the last day of the active clearcut. The first three days were cloudy followed by two days of sunshine.

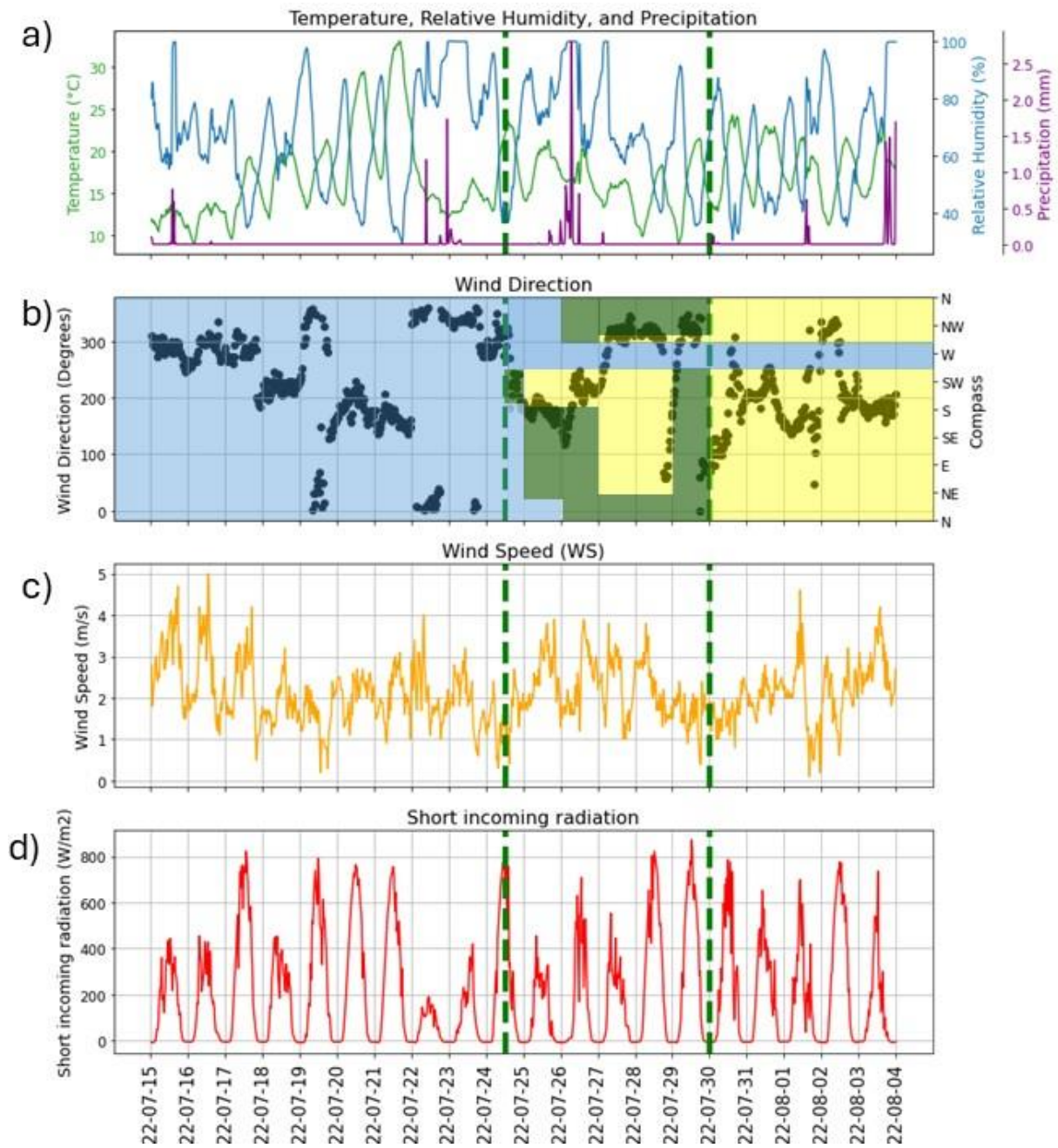


Figure 6: Meteorological parameters at Noranda from 2022-07-15 to 2022-08-04. a) Temperature, relative humidity, and precipitation. b) Wind direction. c) Wind speed. d) Shortwave incoming radiation.

3.2 Effects of the clearcut on monoterpenes, isoprene and sesquiterpenes concentrations

In Figure 7a, the time series of monoterpenes, sesquiterpenes and isoprene measured with the VOCUS PTR are shown. The calculated concentrations of these VOCs were taken from the Master thesis of Chieko Fujimura (Fujimura, 2023). Overall, monoterpenes were the major precursor VOC, followed by isoprene. Sesquiterpene concentrations were very low and often close to zero. When the clearcutting started on the 24th of July monoterpenes concentrations increased and periodic spikes were observed. Monoterpenes and sesquiterpenes concentrations increased almost three times during active-clearcut periods, see figure 7b. Isoprene concentration during the active clearcut showed a decrease of 50 % compared to that during the pre-clearcut period.

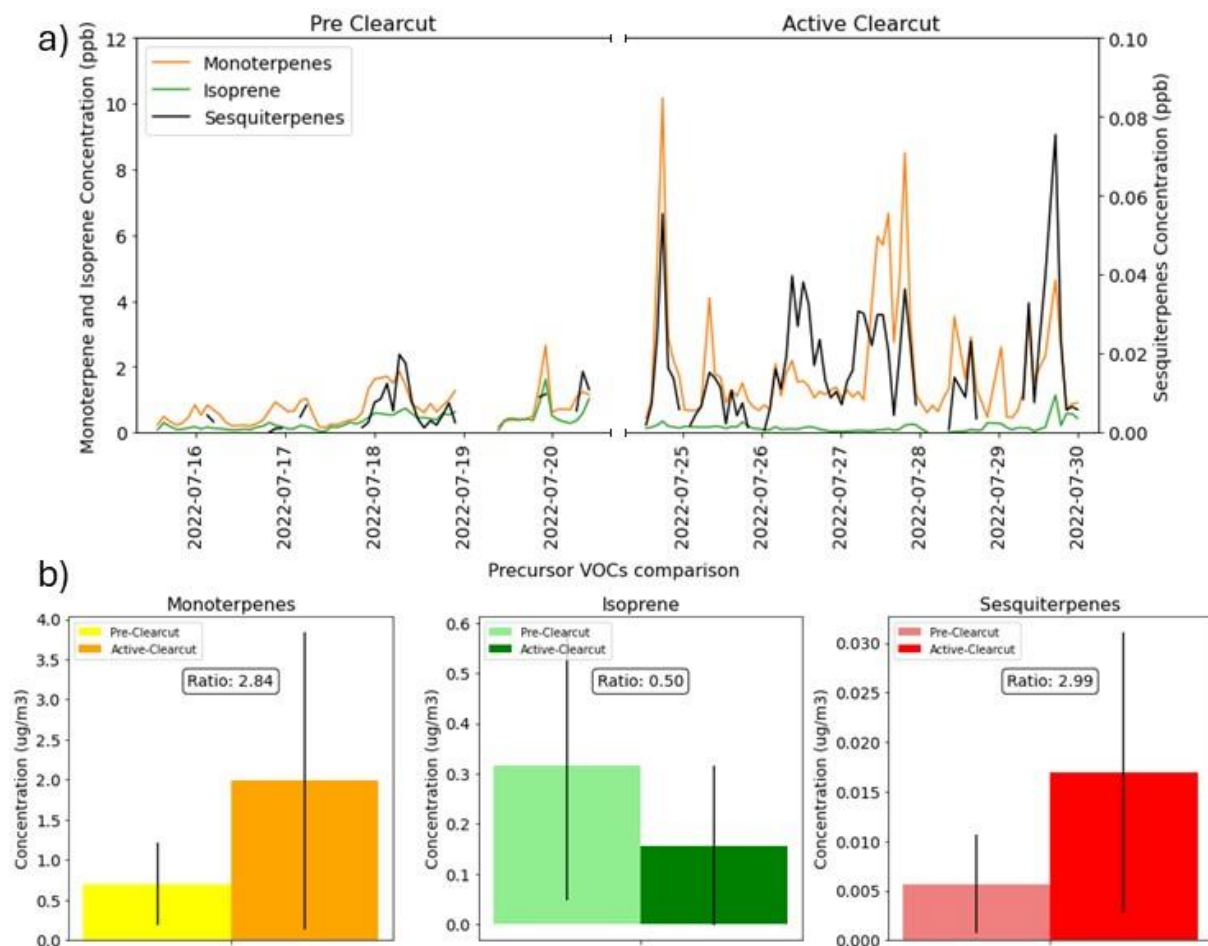


Figure 7: a) Time series of monoterpenes isoprene and sesquiterpenes. b) The average concentrations of monoterpenes, isoprene and sesquiterpenes during the pre-clearcut and active clearcut period. The black bars indicate the variability of the samples.

There were considerable changes in diurnal patterns for monoterpenes and sesquiterpenes. In figure 8 the diurnal pattern of VOC concentrations from both pre-clearcutting period and active clearcutting period are shown. During the pre-clearcut monoterpenes and sesquiterpenes showed lower concentrations during daytime, and higher during evening and night-time. Isoprene concentrations was relative stable during daytime but showed an increase after 20:00. During the active clearcut period, the diurnal patterns (see figure 8b) was reversed for monoterpenes and sesquiterpene as they reached the highest concentrations during the daytime. Isoprene showed a similar diurnal profile as during the pre clearcut but with a lower peak concentration than previous pattern.

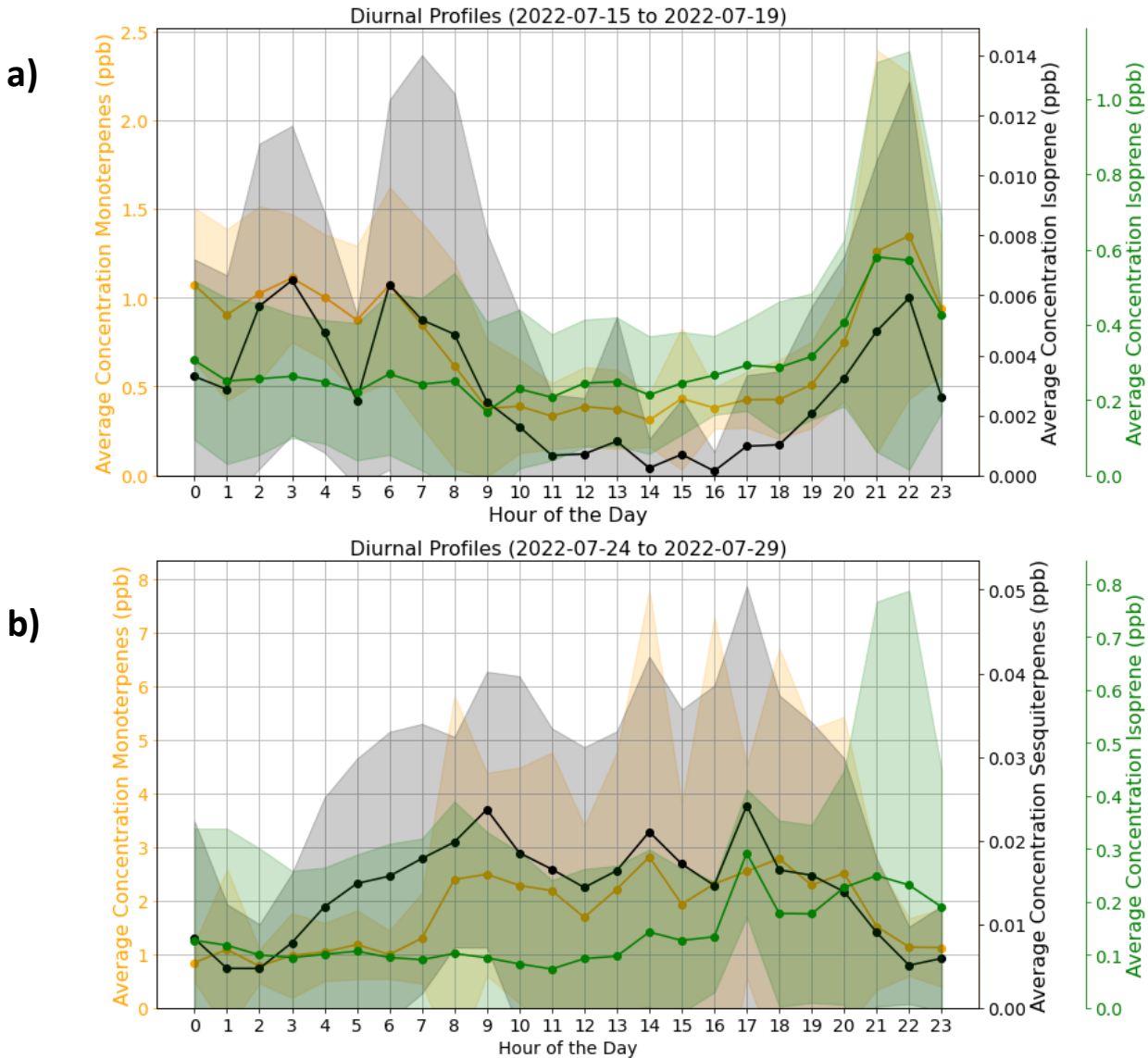


Figure 8: a) Diurnal patterns for monoterpenes, isoprene and sesquiterpenes for pre-clearcut period. b) Diurnal patterns for monoterpenes, isoprene and sesquiterpenes for active-clearcut period.

3.3 Gas and particle distribution during pre-clearcut and active-clearcut period

With the FIGAERO-CIMS data, 380 organic compounds (containing C, H, O and N) within the mass range 60 to 450 m/z were identified. Out of these 380 identified compounds, 79 contained nitrogen. The number of carbon atoms ranged from 1 to 20. The number of oxygens ranged from 2 to 12 going from less oxidized to highly oxidized.

Due to the vast number of different products that can form during oxidation of VOCs (Goldstein & Galbally, 2007) it can be challenging to investigate every single compound separately. One way to manage the large amounts of oxidation products is to group them based on the number of carbons. The products that are formed during oxidation of monoterpenes consist mainly of C₇₋₁₀ compounds and oxidation of sesquiterpenes leads to the formation of C₁₃₋₁₅ compounds. Many products formed during the oxidation of isoprene are likely C₄₋₅ compounds however these can also be due to C-C splitting reactions during oxidation of monoterpenes and sesquiterpenes. Lower carbon containing compounds may also form during thermal decomposition in the particle phase (Barreira et al., 2021).

Of the three types of grouped compounds, C₇₋₁₀ compounds were the largest fraction of identified compounds. C₄₋₅ made up second largest and C₁₃₋₁₅ compounds made up smallest fraction. The entire list for the identified organic compounds is found in appendix table 1.

The top 20 compounds for gas- and particle-phase are found in in figure 9 and 10. Major compounds in gas phase contained a mix of C₇₋₁₀ compounds, C₄₋₅ compounds and C₆ compounds. Major compounds in the particle phase were almost exclusively C₇₋₁₀ compounds. The compounds in gas phase were generally less oxidized than particle phase compounds.

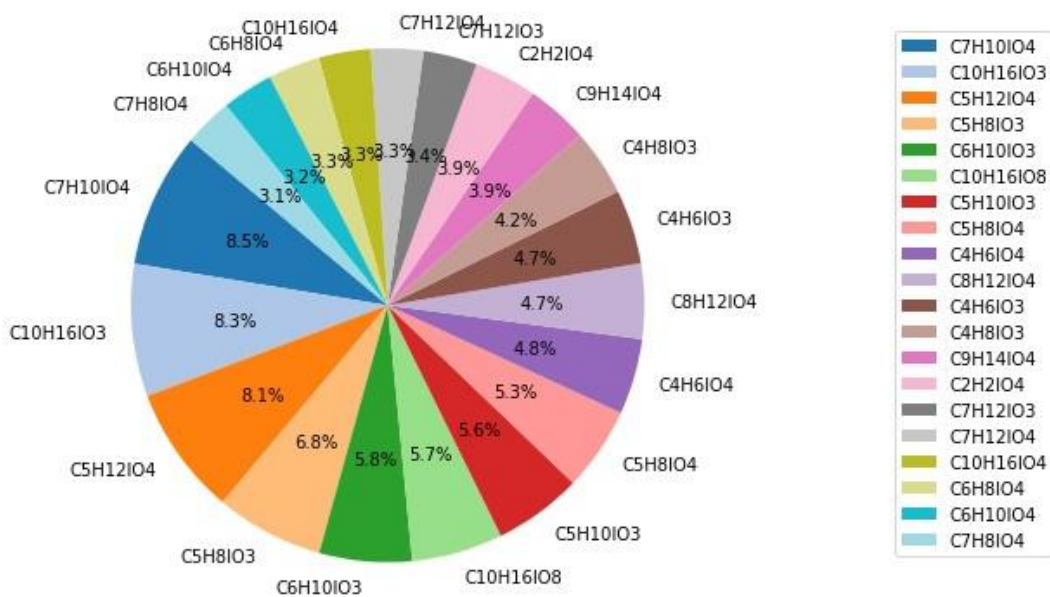


Figure 9: Top 20 compounds in gas-phase during the active clearcut.

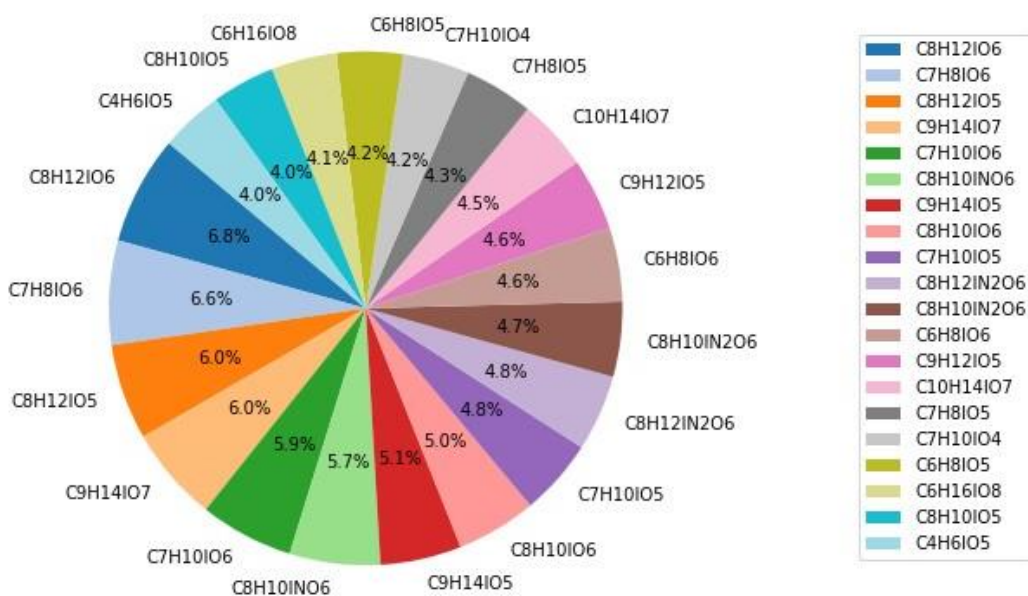


Figure 10: Top 20 compounds in particle-phase during the active clearcut.

Figure 11 show the time series of the total organic compounds in gas and particle-phases measured with the FIGAERO CIMS. Overall, the concentration of total organics in gas phase were higher than concentrations of compounds measured in particle phase.

Both gas- and particle-phase organics started at low concentrations in the pre-clearcut period. They then started increase at the end of the 17th and reached relatively high levels compared to earlier days, during the 18th and 19th of July. During the active clearcut period concentrations were relatively higher for the first two days of the active clearcut. Concentrations then started

to decrease on the 26th of July until they reached concentrations similar to those that was found during the first two days of the pre-clearcut period.

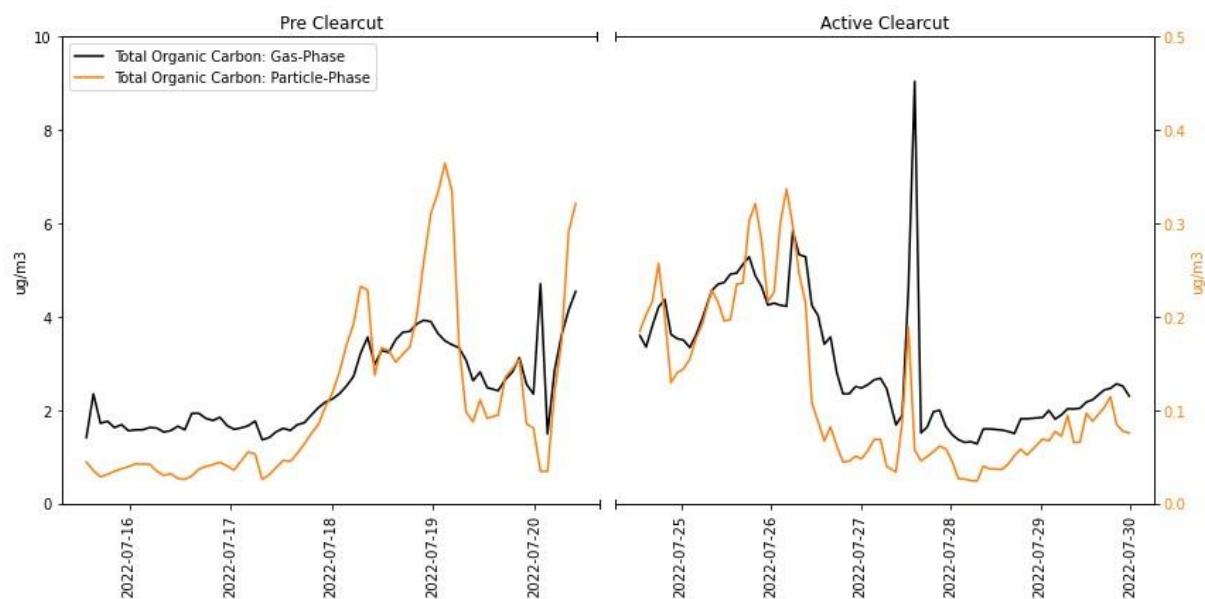


Figure 11: Time series of total amount of organics in gas and particle phase for the pre-clearcut and the active clearcut period.

The time series for the grouped compounds in gas-phase can be seen in Figure 12 a. For gas phase all oxidation product groups showed an increase in concentration during the clearcut, see figure 12 b. The increase did however not correspond to the ratio of increase in the assumed precursor VOCs (see Figure 7b). Monoterpene oxidation products showed the largest increase (37%) in average concentration although the ratio of increase did not match the large increase in monoterpene concentrations. Sesquiterpene oxidation products increased by 25% and Isoprene oxidation products showed an increase in ratio (28%) even though isoprene concentrations instead had been reduced.

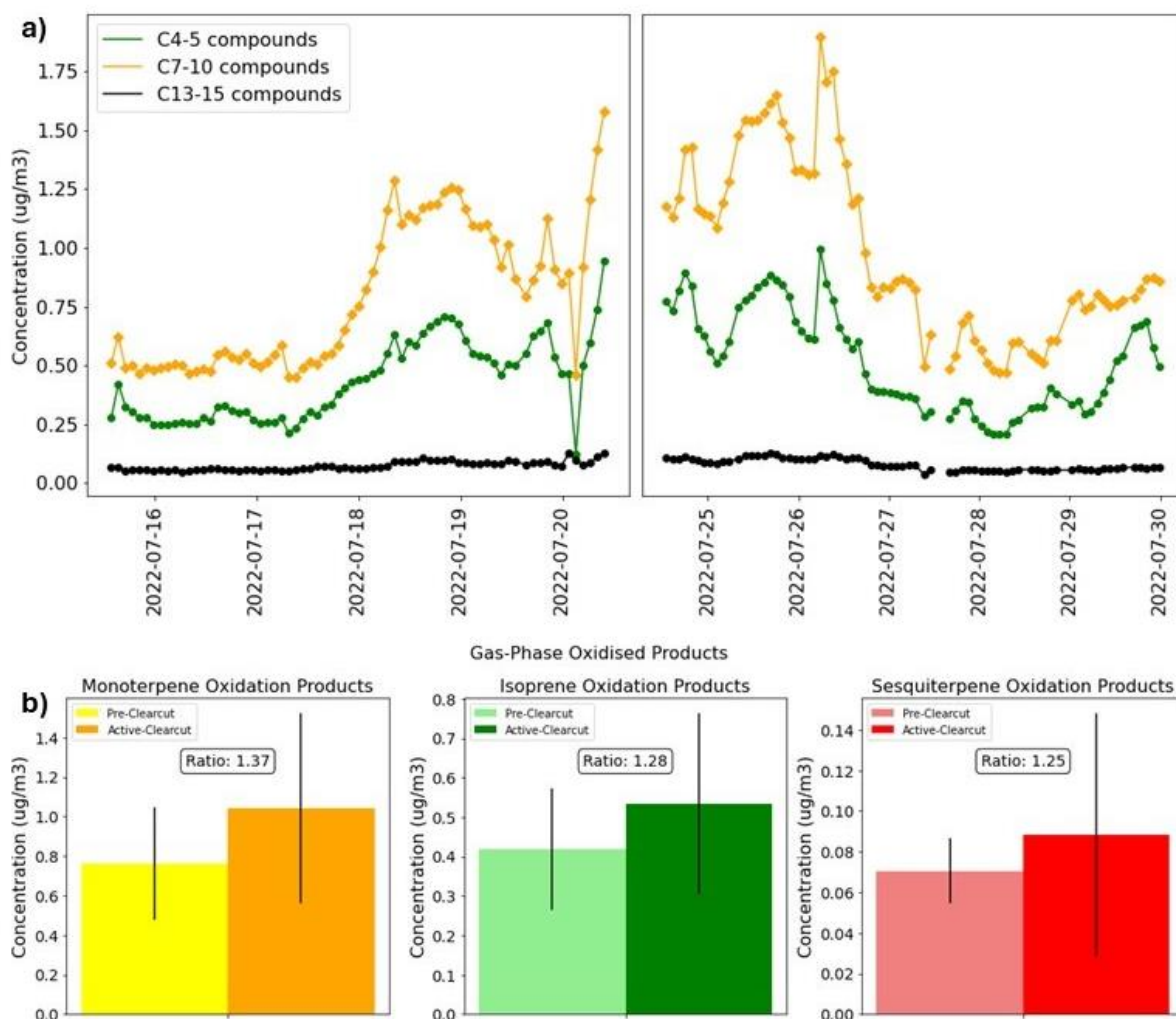


Figure 12: a) Time series for the grouped compounds based on the number of carbons in gas-phase. b) The average concentrations of monoterpene-, isoprene- and sesquiterpene oxidation products in gas-phase during the pre-clearcut and active clearcut period. The black bars indicate the variability of the samples.

The time series for the grouped compounds in particle-phase can be seen in figure 13 a. Overall, the particle-phase compounds showed a similar pattern as that of the gas-phase. All oxidation product ratios increased. Monoterpene oxidation products increased by 17%, isoprene oxidation products increased by 28% and sesquiterpene oxidation products increased by 19% (see Figure 13b).

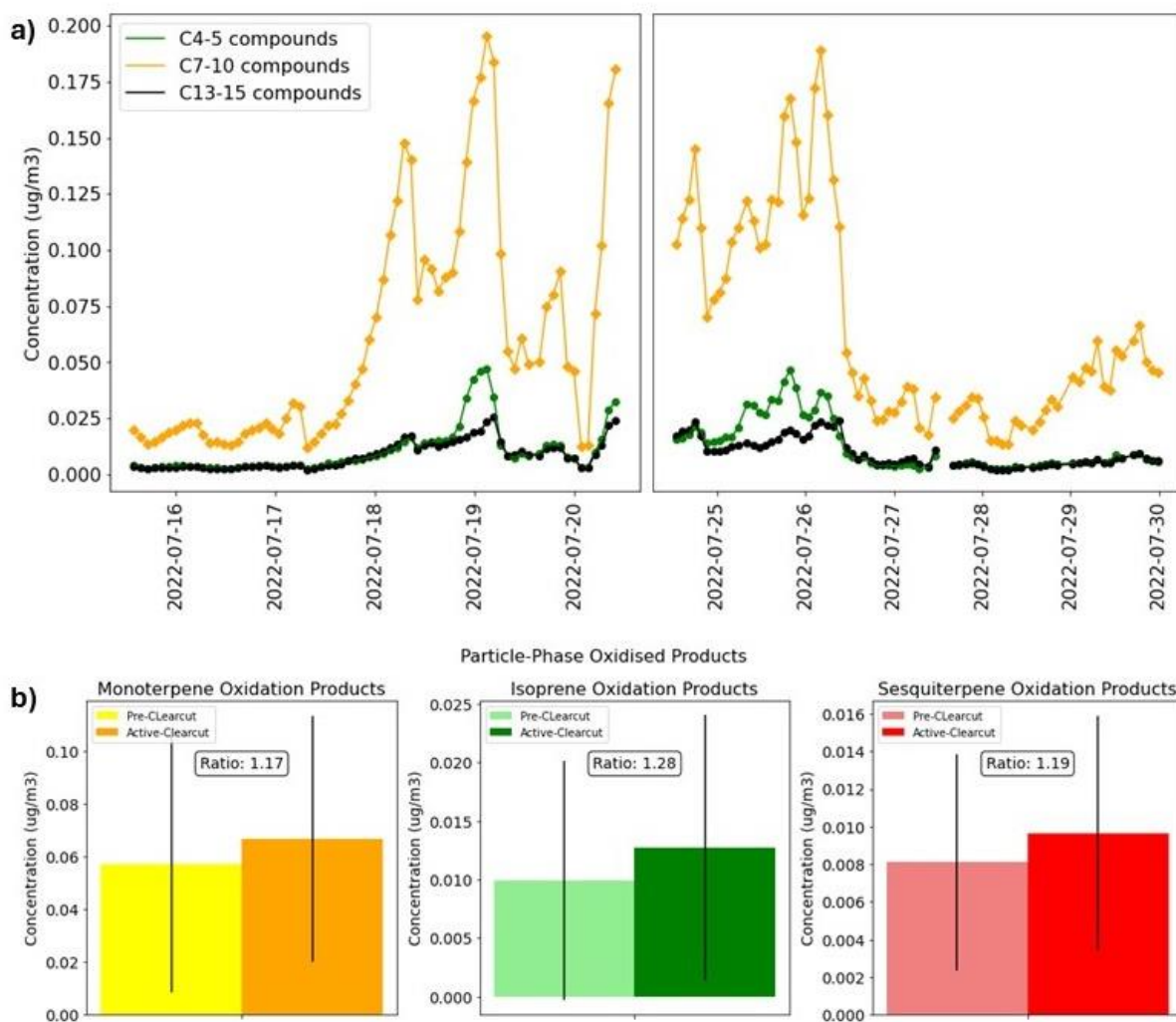


Figure 13: a) Time series for the grouped compounds based on the number of carbons in particle-phase. b) The average concentrations of monoterpene-, isoprene- and sesquiterpene-oxidation products in particle-phase during the pre-clearcut and active clearcut period. The black bars indicate the variability of the samples.

3.4 Composition of gas and particle phase oxidation product

Figures 14, 15, 16 and 17 show the average mass spectrums for the pre-clearcut period (2022-07-15 to 2022-07-20), and active clearcut period (2022-07-24 to 2022-07-29) for gas- and particle-phase respectively. Green bars are C₄₋₅ compounds, yellow bars are C₇₋₁₀ compounds, black bars are C₁₃₋₁₅ compounds and compounds with any other numbers of carbon are purple bars. Gas-phase signals were averaged over each sampling cycles and then averaged again over the pre- and active-clearcut periods. Particle-phase signals were first integrated for each heating cycle and then averaged over pre and active-clearcut. The compounds with the highest signals have markers to indicate which these were.

Looking at the mass spectra for gas-phase, figures 14 and 15, a lot of smaller compounds was observed with some of the major compounds being C₄₋₅ compounds which are likely products

derived from oxidation of isoprene. Some of the higher signals were also from C₇₋₁₀ compounds which are likely products from monoterpenes (Barreira et al., 2021). Most of the more abundant compounds found in gas phase ranged from C₇₋₁₀. The major compounds in the mass spectra for particle-phase (see figures 16 and 17) were mainly C₇₋₁₀ compounds. The changes in gas and particle phase composition when comparing mass spectrums for the pre- and active-clearcut periods were not very large.

See figure S2 in appendix for to see the different types of compounds based on their number of carbons, oxygens, and average measured signal.

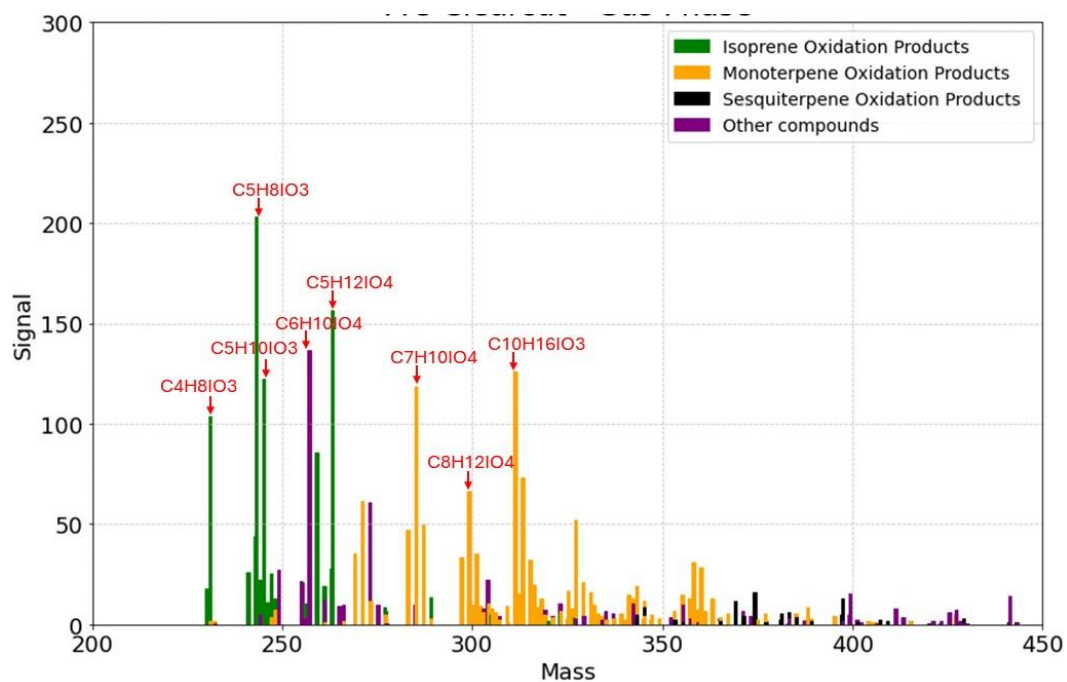


Figure 14: Gas-phase mass spectrum based on the averaged signal during the pre-clearcut period. Major compounds have been marked out.

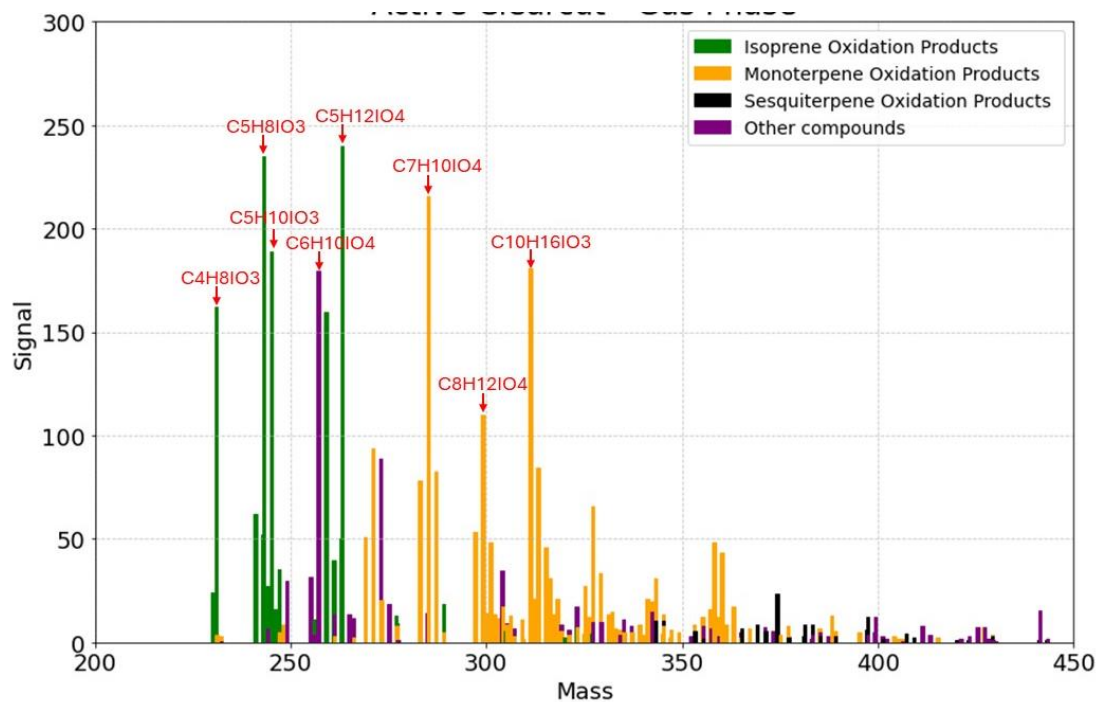


Figure 15: Gas-phase mass spectrum based on the averaged signal during the active-clearcut period. Major compounds have been marked out.

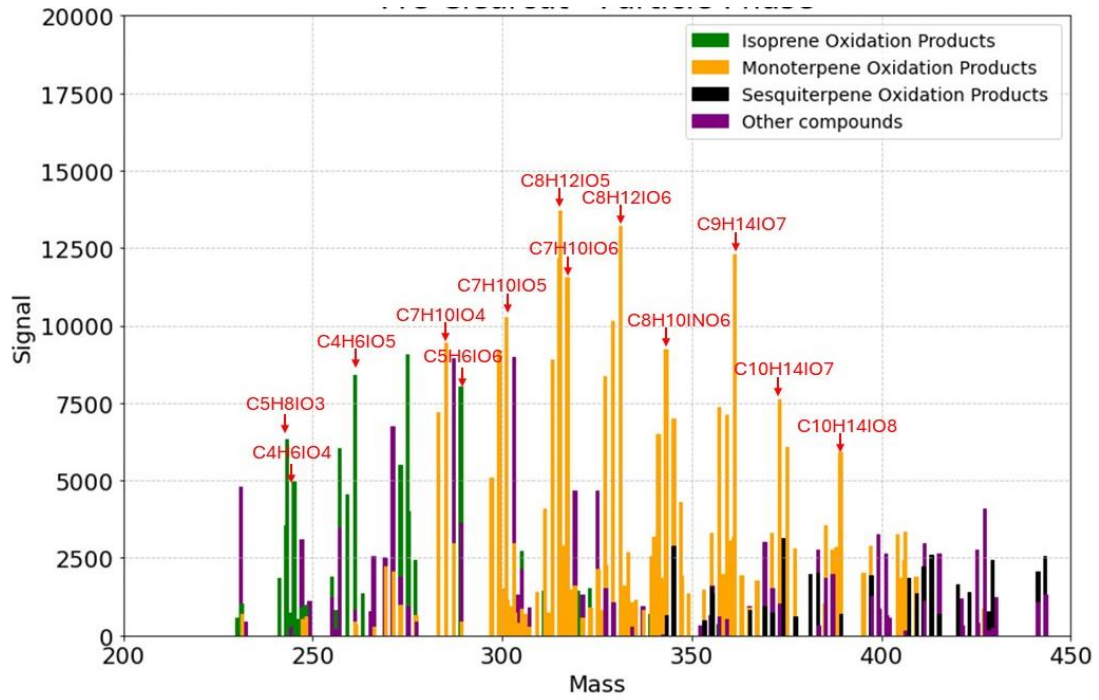


Figure 16: Particle-phase mass spectrum based on the averaged signal during the pre-clearcut period. Major compounds have been marked out.

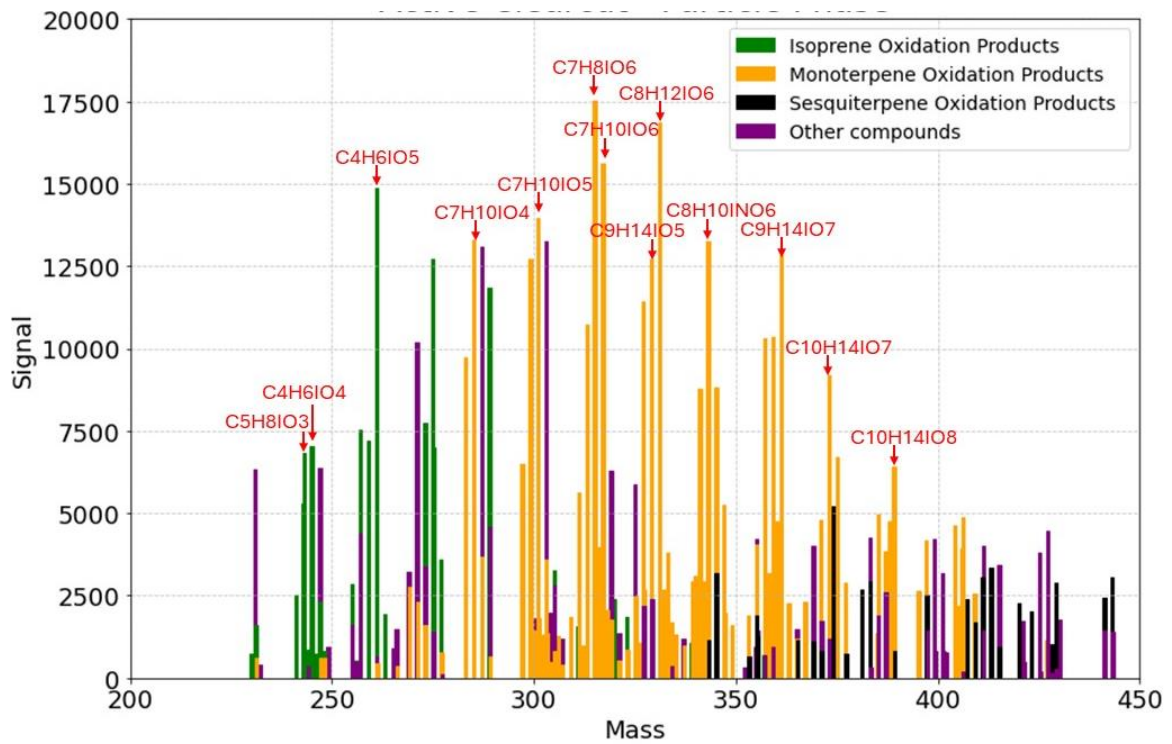


Figure 17: Particle-phase mass spectrum based on the averaged signal during the active-clearcut period. Major compounds have been marked out.

3.5 Impacts of the clearcutting

During the pre-clearcut period, increasing VOC and oxidation product concentrations were observed during warmer temperatures combined with daytime hours (see figure 18). A higher temperature during nighttime hours resulted in increased VOC concentrations but not increased oxidation compounds concentration.

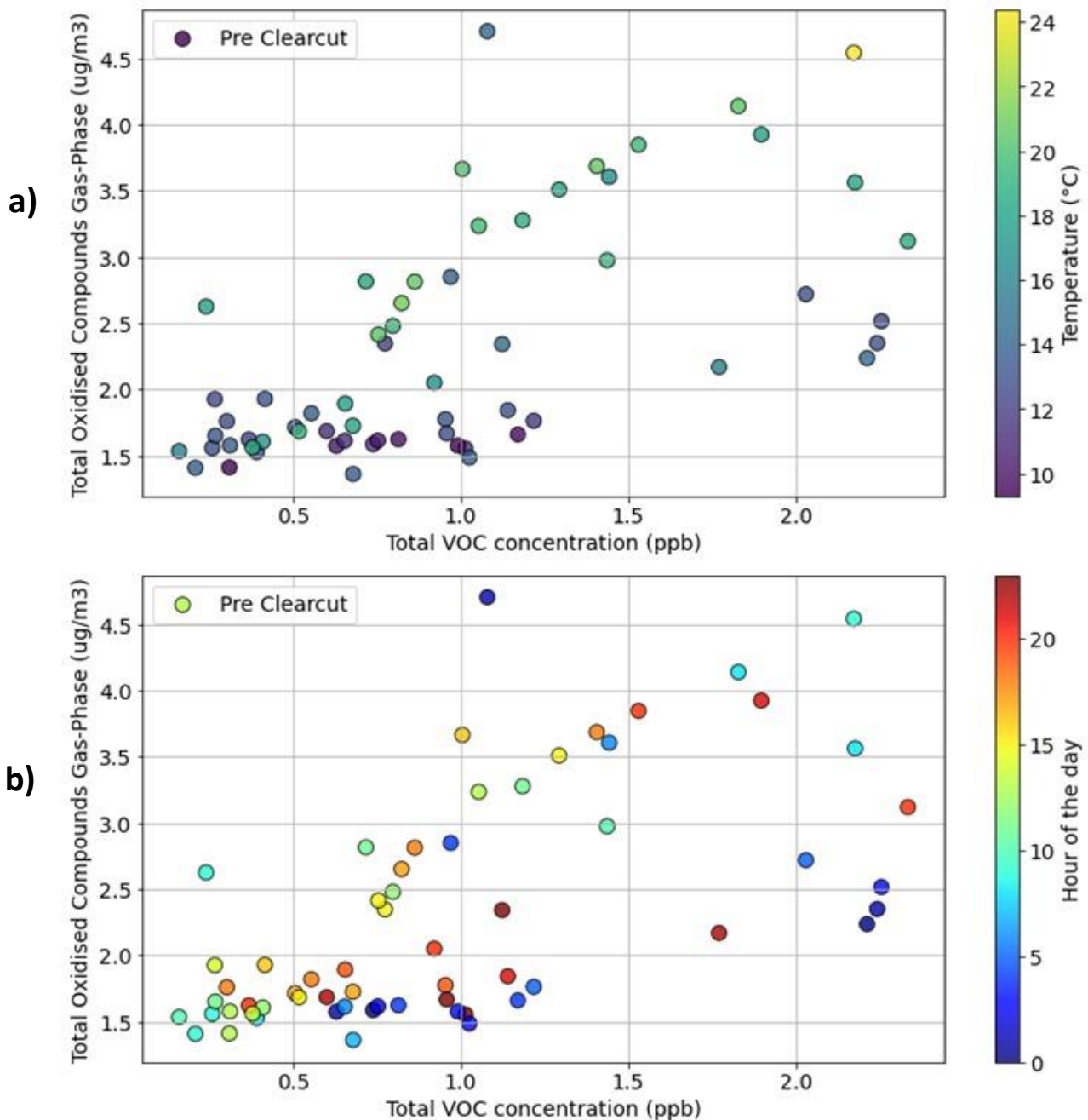


Figure 18: Total oxidised compounds in gas-phase vs total VOC concentrations during the pre-clearcut. a) The colour represents the temperature. b) The colour represents the hour of the day.

In Figure 19 and 20 the total mass concentration of oxidised compounds is plotted against the total concentration of monoterpenes, sesquiterpenes and isoprene for the pre clearcut period and the active clearcut period respectively. The colour of the datapoints indicate what the ambient temperature was. The trend line has been force fitted to zero in gas- and particle-phase to not show a trend for negative total VOC concentration and oxidised products.

For both gas- and particle-phase the pre-clearcut period show a relatively good correlation with total oxidised compounds concentration and the precursor VOCs as indicated by the trendline. However, during the active clearcut period there were more outliers thus the correlation is not as apparent. Increasing VOC and oxidation products concentrations were observed during warmer temperatures combined with daytime hours.

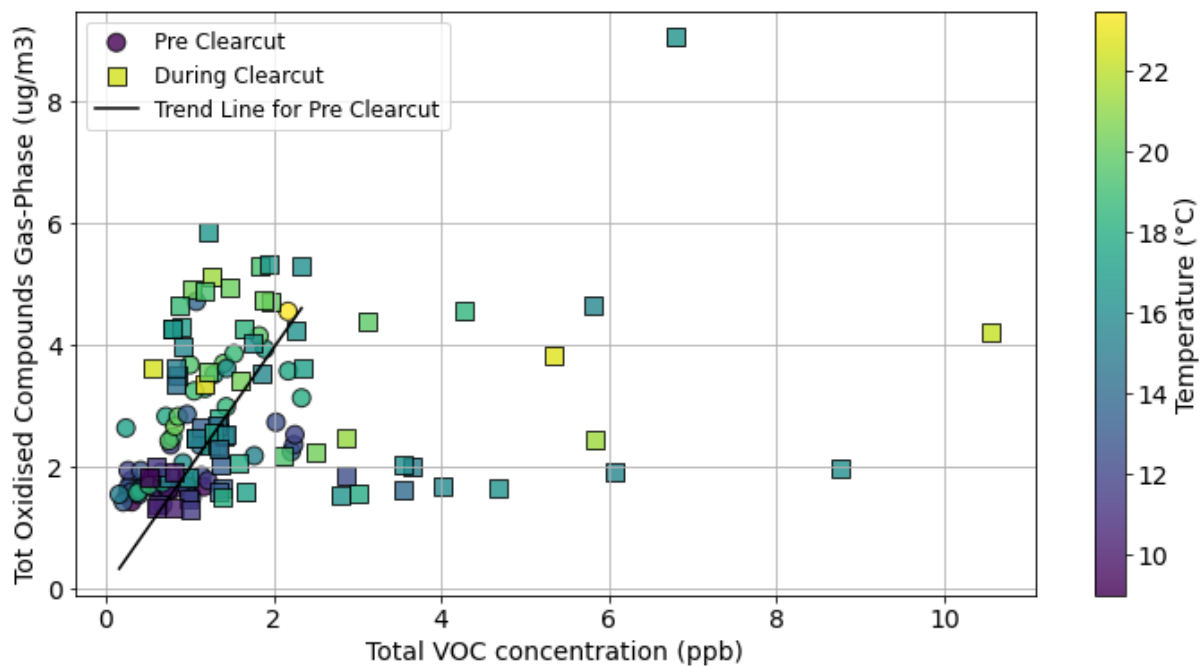


Figure 19: Total amount of oxidised compounds in gas phase vs total amount of the precursor VOCs monoterpenes isoprene and sesquiterpenes. The trendline have been forced through 0.0 as it was assumed that a concentration of 0 ppb precursor VOCs (x-axis) should not contribute to any oxidised products.

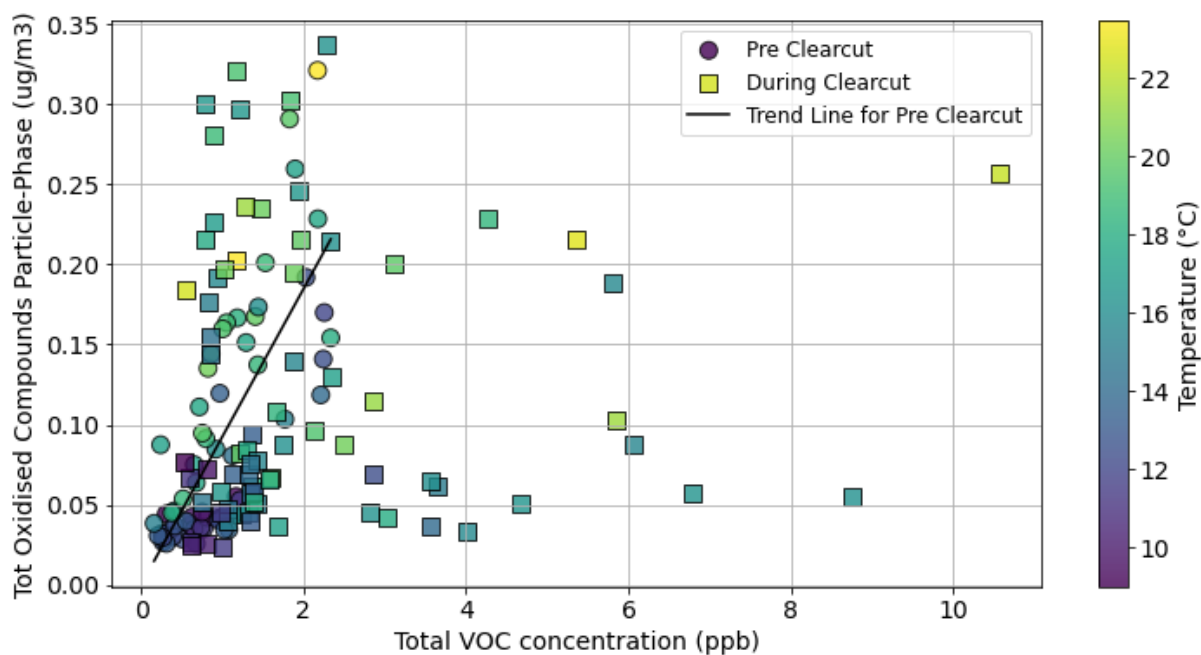


Figure 20: Total amount of oxidised compounds in particle-phase vs total amount of the precursor VOCs monoterpenes isoprene and sesquiterpenes. The trendline have been forced through 0.0 as it was assumed that a concentration of 0 ppb precursor VOCs (x-axis) should not contribute to any oxidised products.

As mentioned previously the changes in gas and particle-phase were small when comparing the mass spectrums for the entire pre- and active clearcut period. However, when comparing individual periods with events of high VOC concentrations and low oxidation products concentrations (HVLO), with events of high VOC concentrations and high oxidation products concentrations (HVHO), the composition of major compounds was different, especially in the gas-phase (see Figures 20 and 21). These mass spectrums were based on events that occurred during the outliers in figure 18. $C_5H_6O_3$ was the largest contributor to gas phase during HVHO. $C_5H_6O_3$ have been proposed to be formed during from H-abstraction of C_5H_6O which is an isoprene oxidation product (D. Wang et al., 2022). Apart from $C_5H_6O_3$ the contribution of isoprene oxidation products to the total amount of oxidised products was lower in HVHO compared to that of HVLO. Another compound that showed a large increase during HVLO was $C_{10}H_{16}O_3$ and has been reported as a monoterpene tracer for OH and O_3 oxidation. (Zhang et al., 2018).

Looking at the pattern of the mass spectrums in Figures 21 and 22 there are similarities between them, and monoterpene oxidation products tends to be the overall largest contributor in both cases. There are some shifts in what the major compounds were and apart from $C_5H_6O_3$ the contribution of isoprene oxidation products to the total amount of oxidised products was lower in HVHO compared to that of HVLO.

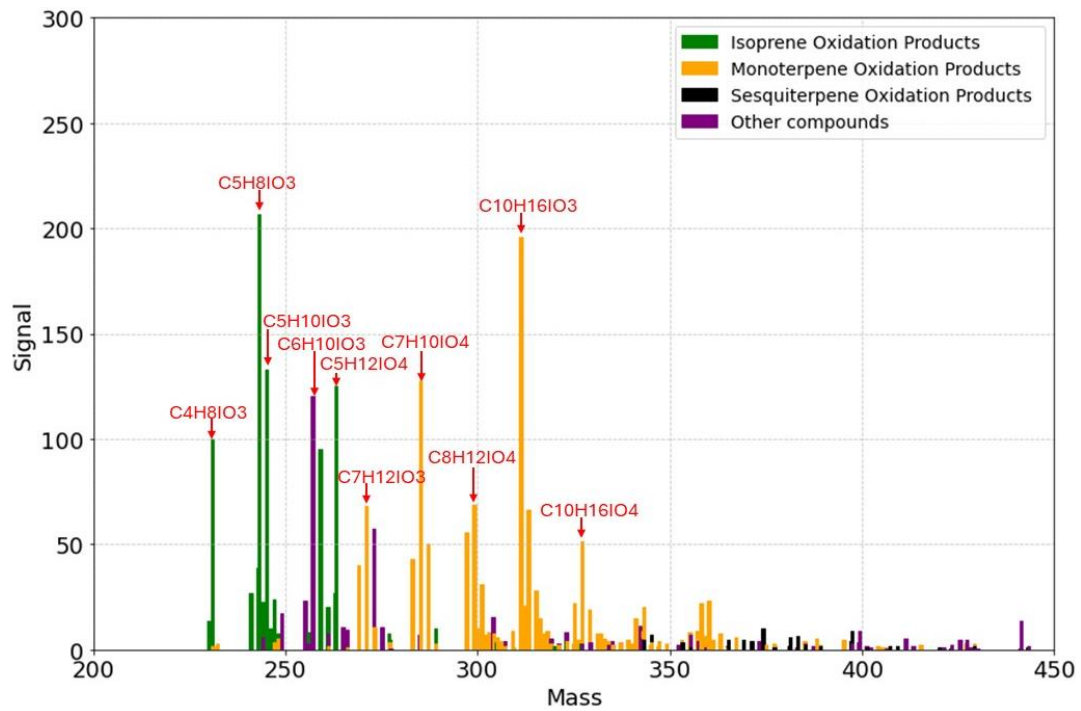


Figure 21: Gas-phase mass spectra during high VOC concentration (8,3 ppb) and low oxidation products concentration (1.9 $\mu\text{g}/\text{m}^3$)

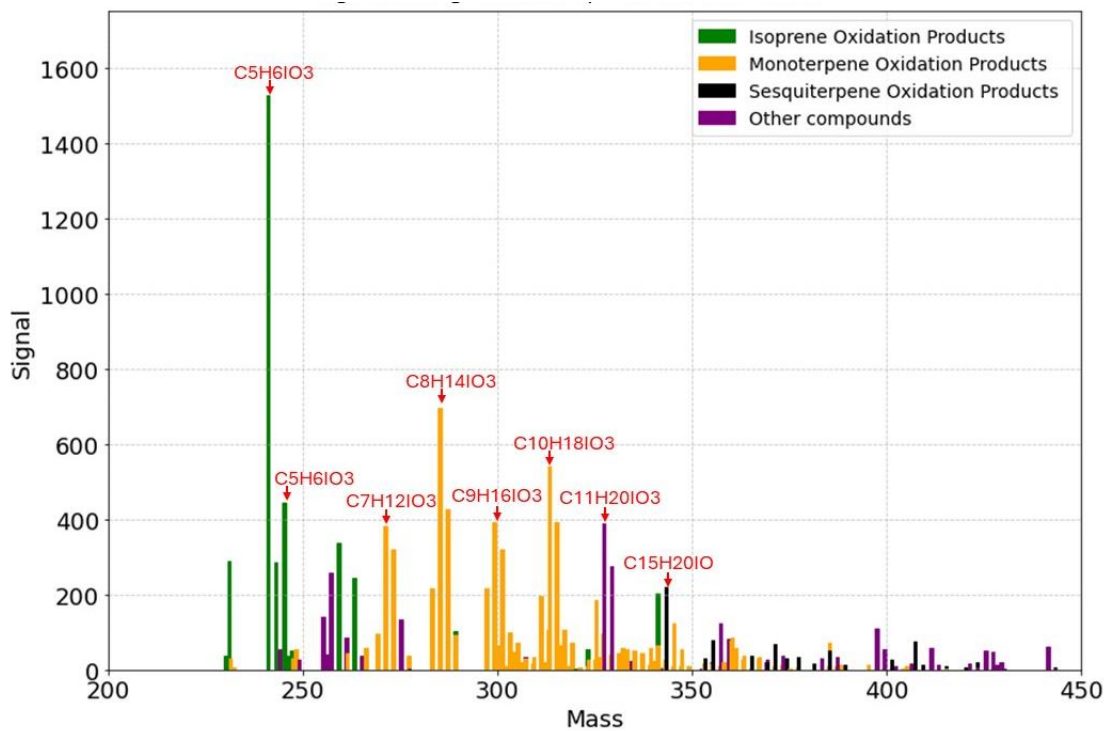


Figure 22: Gas-phase mass spectra during high VOC concentration (6,4 ppb) and low oxidation products concentration (9.9 $\mu\text{g}/\text{m}^3$)

In addition, the grouped compounds were plotted against their suspected precursor VOC to compare their correlation before and during the active clearcut (see figure 23 and 24). Isoprene oxidation compounds, C₄₋₅ compounds, increased more rapidly with increasing isoprene concentration during the pre-clearcut (black datapoints Figure 24 a and b) than during the active clearcut (yellow datapoints in Figure 24 a and b) in both gas and particle phase. Monoterpene oxidation products, C₇₋₁₀ compounds, showed the opposite trend as there was a relatively good correlation with increasing monoterpene levels during the pre-clearcut (black datapoints Figure 23 a and b). However, despite higher concentrations of monoterpenes during the active clearcut oxidation products did not increase correspondingly but remained at lower concentrations (yellow datapoints figure 23 a and b). This effect for monoterpene oxidation products was observed in both gas and particle phase.

When sesquiterpene oxidation products, C₁₃₋₁₅ compounds, was plotted against sesquiterpenes there was a relatively poor correlation especially during the pre-clearcut (not shown in the figure below). This was likely due to sesquiterpene concentrations being very low, often close to 0, thus there were not many datapoints to check correlation that could be plotted.

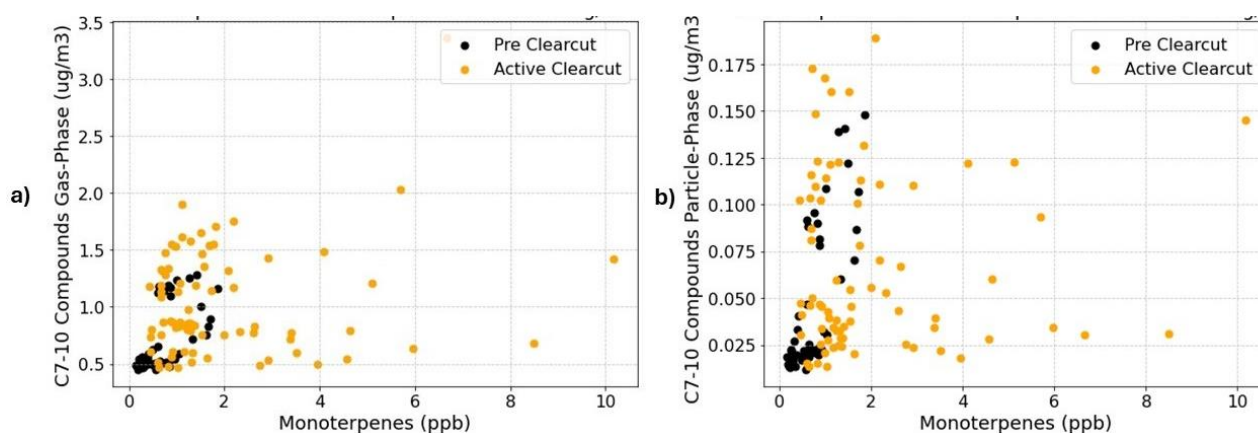


Figure 23: a) C7-10 compounds in gas-phase vs monoterpenes. b) C7-10 compounds in particle-phase vs monoterpenes.

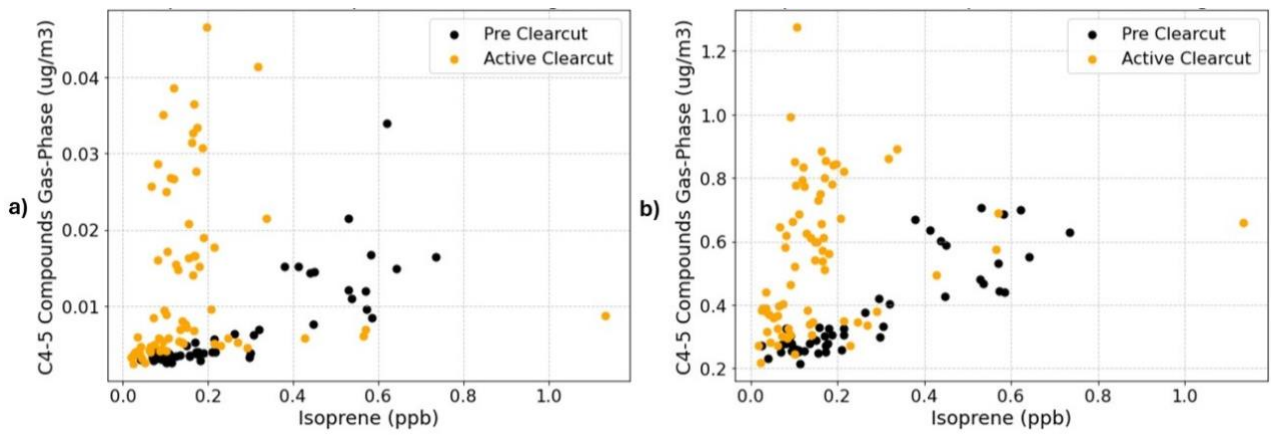


Figure 24: a) C4-5 compounds in gas-phase vs monoterpenes. b) C4-5 compounds in particle-phase vs monoterpenes

4 Discussion

4.1 Metrological parameters

There are many parameters affecting VOC emissions, and their chemical and photochemical oxidation in the atmosphere. Meteorological parameters such as temperature, relative humidity, precipitation, wind direction and wind speed are some that were considered in this project.

Temperature can affect BVOCs emissions in two ways. Firstly, an increase in temperature up to 40 °C may lead to increased activity of enzymes responsible for BVOCs biosynthesis (Hüve et al., 2011). Secondly, increased temperature may also lead to increased evaporation of BVOCs from storage pools (Loreto & Schnitzler, 2010). Light will increase the production of BVOCs through *de novo* synthesis until it reaches a point of light saturation (X. Wang et al., 2022). Wind direction and wind speed will affect what source that is measured and the amount of dilution that occurs. (Y. Liu et al., 2019). Relative humidity affects the formation of water films on leaves and soils which can inhibit the evaporation of VOCs (Mäki et al., 2019). Precipitation can have a scavenging effect and thus rain can lead to decreased BVOC concentrations (Sato et al., 2006).

The first period of the clearcutting occurred for six days where different areas around the flux tower at the site were being worked on each day. As already described the wind direction is an important factor that needed to be considered. If the wind was blowing from the wrong direction species emitted due to the clearcut would not be measured, since they would not reach the sample inlets at the tower. In addition, the areas that were being worked on during the clearcutting was not always the same size. Therefore, trying to estimate how much of the measured species originated from the clearcut proved to be difficult. However, as described in figure 8, the wind direction was for the most part coming from either, a part that was actively being worked on that day (green area), or from an area that had been worked on a previous day (yellow area). Thus, the measured species should at least in part be considered to originate from the clearcut areas although there are uncertainties in the fraction. Ideally measurements would contain only species that are emitted due to the clearcut, however since only a very small area was clearcut compared to the surrounding forest the identified compounds and their measured concentrations is likely a mix of species that are produced during a clearcut and coming from the areas that had not been clearcut.

Temperature and time of the day both affected total VOC concentrations total amount of oxidation products during the pre-clearcut period as shown in figure 18. During daytime hours

increased temperature correlated well with increasing VOC concentration and increasing total oxidation product concentrations. During night-time and early morning an increase in temperature generally caused higher VOC concentrations but not higher total oxidation products concentrations. OH, and O₃ are the major oxidants during daytime (Han & Jang, 2023) and thus this indicates that OH and O₃ oxidation were the most important oxidation pathways during the Norunda clearcut.

As shown in figure 8 the diurnal patterns of monoterpenes and sesquiterpenes changed. During the pre-clearcut period monoterpene concentrations were greater during night-time. This was likely since monoterpenes concentrations are oxidised during daytime. The loss of monoterpenes through oxidation is greatest during daytime, and monoterpene OH oxidation is the main cause of loss during daytime. (H. Wang et al., 2022). The increase of monoterpenes and sesquiterpenes daytime concentrations during the active clearcut (see Figure 8b) could be due to oxidant limitations. During the active clearcut the total VOC concentrations increased significantly. There may not have been enough OH to oxidise the large increase in total VOC and hence an increase in monoterpenes and sesquiterpenes are observed during daytime of the active clearcut.

4.2 The effect of clearcutting on monoterpenes, sesquiterpenes and isoprene emissions

The main type of BVOCs that are emitted from boreal forests are isoprene, monoterpenes and sesquiterpenes. The type of BVOC emitted is not always the same and can differ within a species. However, species in the same given area generally emit the same BVOCs. (Vestenius et al., 2021). The result of this study confirms this, and that especially monoterpenes and isoprene are important BVOCs emitted from boreal forests.

One of the main effects of the clearcut that can be seen by looking at the time series for precursor VOCs (see figure 7a). There is a high variability in concentrations, but they were generally lower during the pre-clearcut. During the active clearcut high spikes in concentrations of monoterpenes occurs more frequently. Monoterpene emissions from boreal forest stems from two process, either *de novo* synthesis or evaporation from storage pools (Ghirardo et al., 2010). Oleoresin is a substance that in mature trees can be of significant amount. Between 20-50% of oleoresin is comprised of monoterpenes. Mechanical damage causes the oleoresin to be extruded at the damaged area and when exposed to the atmosphere BVOC such as monoterpene starts to evaporate leaving a resin as a protective layer (Vanhatalo et al., 2015). The spikes in

monoterpenes could thereby be explained by the fact that monoterpene emissions are due to the mechanical wounding to trees that the clearcutting causes.

The other major observed effects of the clearcut were that isoprene decreased by almost half. In contrast to monoterpenes isoprene is emitted only directly after synthesis because it is not stored within the tree resin (Ghirardo et al., 2010). Part of the decrease could possibly be explained by the fact that isoprene is light dependant and produced during *de novo* synthesis. Once the trees are cut down the production of isoprene might therefor stop or at least diminish. The removal of trees should lead to shrubs on the ground receiving lighter as they are no longer shaded by the tree crowns. This could probably lead to increased isoprene production. However, the heavy machinery will also crush much of this shrub vegetation. If this is the only reason for the quite significant decrease in isoprene is not well established but may be part of the explanation for the decrease in isoprene.

4.3 Major oxidation compounds in gas and particle phases

When analysing the major oxidation products in both gas and particle phases (see figure 9 and 10) many of them have been found in previous studies. For instance, $C_7H_{10}O_4$ was the largest contributor to gas phase composition during the active clearcut. This is likely a limonene or α -pinene oxidation product (Dbouk et al., 2024). $C_{10}H_{16}O_3$ also contributed significantly to gas phase. This is likely pinonic acid produced through either ozonolysis or OH oxidation of monoterpenes (Zhang et al., 2018). $C_5H_{12}O_4$ is a previously known SOA tracers for isoprene epoxy diols (IEPOX) (D'Ambro et al., 2017). $C_5H_8O_3$ has been proposed to be produced through isoprene OH oxidation (Liu et al., 2016).

Most of the major compounds found in particle phase are compounds reported previously as monoterpene oxidation products. $C_8H_{12}O_6$ is likely a monoterpene oxidation reported as 3-Mehtyl-1,2,3-butanetricarboxylic acid (MBTCA) (Kristensen et al., 2014). $C_8H_{12}O_5$ likely produced from OH oxidation of either α -pinene or Δ^3 -carene (D'Ambro et al., 2022). $C_9H_{14}O_6$ have previously been reported as being produced during β -pinene ozonolysis (Liu et al., 2023).

The average mass spectra for the entire pre- and clearcut-periods did not show a very large difference in patterns (see figures 14 to 17). This suggests that the clearcut did not change the composition overall. However, the mass spectra's during HVLO and HVHO did show a difference in patterns with higher monoterpene oxidation products concentration which indicates that the clearcut leads to more of these products during certain events.

4.4 Distribution of oxidation products in the gas and particle phase

Assumed products from monoterpenes were dominant in both gas and particle phase, as can be seen in figure 12a and 13a, for both periods. The gas phase concentrations were significantly higher than the measured particle phase concentrations. The use of Teflon tubing often leads to losses in charged particles (X. Liu et al., 2019). This combined with the fact the Teflon line was quite long, 35 meters up into the tower, could be one of the reasons that the total particle concentrations were so much lower than the gas-phase concentrations.

The contribution to the total signals from isoprene oxidation products was found to a higher degree in the gas phase while the contribution to the total signals from the sesquiterpenes oxidation products were found to a higher degree in the particle phase. The volatility of a compound which determines if it will prefer to exist in gas or particle phase will depend the size of the molecule and on the functional groups attached to the carbon chain (Goldstein & Galbally, 2007). It therefore is reasonable that the assumed isoprene products are found to a higher degree in the gas phase than in particle phase as C₄₋₅ compounds have a relatively low mass.

4.5 Oxidant limitations

As already discussed, monoterpenes and sesquiterpenes increased during the active clearcut while isoprene decreased (see Figure 7b). However, oxidation products from monoterpenes, isoprene and sesquiterpenes all increased (see figures 12b and 13b).

The total organics was plotted vs the monoterpene concentrations (see figures 19 and 20). This showed that before the clearcut, total oxidised compounds showed a reasonably good correlation with total VOC concentrations. However, during the active clearcut although total VOC increased significantly the total oxidised compounds did not increase and instead levelled out when monoterpene concentrations increased. Additionally, the monoterpene and sesquiterpene oxidation products did not increase to the same degree as the precursor did. For instance, C₇₋₁₀ only increased by 37% in the gas phase and 17% in the particle phase compared to monoterpenes that increased by 282%. This led to the question why oxidation products were not increasing at the same rate as the precursor VOC.

To investigate this further I looked at how the grouped compounds correlated with their assumed precursor VOC (see figures 23 and 24). The C₄₋₅ compounds showed a steeper slope during the active clearcut period (yellow datapoints figure 24) than during the pre-clearcut period (black datapoints figure 24). The C₇₋₁₀ compounds showed a reversed behaviour where

a steeper slope was observed during the pre-clearcut period (black datapoints figure 23) than during the active-clearcut period (yellow datapoints figure 23). Additionally, the correlation between C₇₋₁₀ compounds concentration and monoterpene concentrations was worse during the active clearcut period. This indicated that increased monoterpene emissions did not lead to increased C₇₋₁₀ oxidation products, at least not to the same extent.

Isoprene shows high reactivity towards OH ($10.1 \times 10^{-11} \text{ cm}^3 \text{ molecule}^{-1} \text{ s}^{-1}$) (Rinne et al., 2012). α -pinene which is one of the major monoterpene compounds emitted from boreal forests (Raisanen et al., 2009) show slightly lower but similar reactivity towards OH ($10.1 \times 10^{-11} \text{ cm}^3 \text{ molecule}^{-1} \text{ s}^{-1}$). During clearcutting with much higher monoterpene emissions, the oxidation of isoprene was expected to be limited by the competition of oxidants. However, there was an increase in isoprene oxidation while isoprene concentrations decreased.

Here, we assume all C₄₋₅ compounds are from isoprene oxidation. Such grouping of compounds based on the number of carbon atoms they contain can simplify the analysis (Yee et al., 2018), (Chan et al., 2011), (Kundu et al., 2017), (Hammes et al., 2019), (Zhang et al., 2018), (Hamilton et al., 2011). It may cause some uncertainties as some of the grouped compounds may be attributed to the wrong type of precursor VOC.

4.6 Further climate impacts

BVOC emissions effects ozone production in the troposphere, hydroxyl radical formation, carbon monoxide levels, lifetime of methane and SOA formation (Ghirardo et al., 2010). This highlights other impacts that clearcutting have on climate. The result of this thesis indicates that not only does clearcutting effect BVOC emissions but also oxidant concentrations since diurnal patterns changed. Since isoprene, monoterpenes and sesquiterpenes all are unsaturated they will react with all the major oxidants (Bergström et al., 2014). The drastic increases in monoterpenes and sesquiterpenes could lead to a direct effect on the oxidation and aging of other species. Meanwhile, VOCs may also influence ozone production. RO₂ and HO₂ produced from OH oxidation of VOCs (reaction 12 and reaction 14) can react with NO which will produce NO₂ (reaction 13 and reaction 15). This can affect the steady state of ozone (see section 1.2.2) and lead to an increased ozone production (Nelson et al., 2021). The extent that certain VOCs have on enhanced ozone formation differs and depends on concentration, reactivity, and the structure of the VOC (Jenkin et al., 2017).





The effect of the clearcut may influence the initial availability of oxidants, but oxidants are also reformed during reactions that follow the initial oxidation of the VOCs. Based on measurements presented here it is not possible to quantify the exact effect that clearcutting have on the oxidative capability of the region. Further effects of forest management on climate could be an important topic for future research. The gross logging in Sweden have increased steadily since the 1950s, see figure 25 (Skogsstyrelsen, 2022). Therefore, the effects that forest management in Sweden have on climate, in addition to SOA formation, will likely become increasingly important.



Figure 25: Plot showing the gross logging each year since 1950 to 2020. Gross logging refers to the volume of all logs including logs which has not been used for production. Data for 2021 is preliminary and 2022 is a prognosis. Unit of the x-axis is in million m³ forest. Plot taken from (Skogsstyrelsen, 2022).

5 Conclusions

The goal of this thesis was to investigate how clearcutting affects BVOC emissions and oxidation products. This was done by analysing and identifying BVOC concentrations and their oxidation products in both gas and particle phases.

Generally, BVOC concentrations were affected by temperature and incoming sunlight. The combined effects of meteorological parameters likely play an important role during emission and oxidation of BVOCs from boreal forests. Of the three precursor BVOC groups investigated here, monoterpene and sesquiterpenes increased while isoprene decreased during clearcutting. Monoterpenes was the dominant precursor BVOCs both before the clearcut and during the clearcut. Their oxidation products were also dominant in both gas- and particle-phase. The main effect that was seen during clearcutting was that monoterpene and its oxidation products increased. Furthermore, clearcutting affected diurnal patterns of the precursor VOCs and lead to enhanced contribution to particle formation.

Finally, clearcutting being the most common method of forest harvesting combined with the fact that gross logging has and continuous to increase, will likely lead to increased BVOC emissions and SOA formation in the future. Further research on the topic is needed to fully assess the impacts that clearcutting may have on regional air quality and climate.

6 Appendixes

6.1 Table 1: Identified oxidised organic compounds.

Molecular Formula	Mass	Oxygen to carbon ratio
CHO3	61.02	3
CH2IO2	172.93	2
CH4IN2O	186.96	1
CH3INO2	187.94	2
CH4IN2O2	202.96	2
C2H3O2	59.04	1
C2H6IN2O4	248.98	2
C2H4IO4	218.96	2
C2H5IO3	203.96	1.5
C2H7IN2O5	265.99	2.5
C2H6IN2O7	296.98	3.5
C2H2IO4	216.94	2
C2H2IO3	200.94	1.5
C2H4IO2	186.96	1
C2H4IO3	202.96	1.5
C2H5IO2	187.96	1
C3H6IO2	200.98	0.67
C3H4IO4	230.97	1.33
C3H6IO6	264.98	2
C3H8IO3	219	1
C3H4IN2O4	258.98	1.33
C3H6IO3	216.98	1
C3H4IO5	246.97	1.67
C3H7IO6	265.99	2
C3H9IO	188.01	0.33
C3H4IN2O8	322.98	2.67
C4H9IO4	248.02	1
C4H8IO4	247.01	1
C4H6IO8	308.99	2
C4H8IO8	311.01	2
C4H10IN2O3	261.04	0.75
C4H6IO5	260.99	1.25
C4H8IO5	263.01	1.25
C4H6IO6	276.99	1.5
C4H4IO6	274.98	1.5
C4H8IN2O3	259.02	0.75

C4H7IO4	246	1
C4H8IO9	327.01	2.25
C4H6IO4	244.99	1
C4H8IN2O7	323.02	1.75
C4H4IO4	242.98	1
C4H6IO3	228.99	0.75
C4H8IO3	231.01	0.75
C4H7IO3	230	0.75
C5H12IN2O2	259.07	0.4
C5H11IO2	230.04	0.4
C5H6IO7	305	1.4
C5H10IO4	261.04	0.8
C5H10IO3	245.04	0.6
C5H8IO5	275.02	1
C5H10IN2O4	289.05	0.8
C5H6IO8	321	1.6
C5H11I2O2	356.95	0.4
C5H12IO4	263.05	0.8
C5H6IO5	273	1
C5H8IO4	259.02	0.8
C5H7INO7	320.02	1.4
C5H10IO9	341.03	1.8
C5H11IO3	246.04	0.6
C5H9IO3	244.03	0.6
C5H8IO3	243.02	0.6
C5H6IO6	289	1.2
C5H14IO7	313.06	1.4
C5H6IO3	241	0.6
C5H10IO7	309.03	1.4
C5H12IN2O6	323.06	1.2
C5H4IO4	254.99	0.8
C5H7INO3	256.02	0.6
C5H10IO5	277.03	1
C5H6IO4	257	0.8
C5H8IO9	339.02	1.8
C6H6IO7	317.01	1.17
C6H10IO5	289.05	0.83
C6H9IO6	304.04	1
C6H7INO5	300.03	0.83
C6H8IO8	335.03	1.33
C6H6IO6	301.01	1

C6H5IO7	316	1.17
C6H7IO8	334.02	1.33
C6H10IO7	321.04	1.17
C6H8IO6	303.03	1
C6H10IO6	305.04	1
C6H12IO6	307.06	1
C6H8IO5	287.03	0.83
C6H14IO7	325.08	1.17
C6H10IO8	337.04	1.33
C6H6IO5	285.01	0.83
C6H8IO7	319.03	1.17
C6H10IO4	273.05	0.67
C6H6IO4	269.01	0.67
C6H9IO3	256.04	0.5
C6H14IO3	261.08	0.5
C6H16IO8	343.09	1.33
C6H12IO4	275.06	0.67
C6H8IO3	255.03	0.5
C6H12IO9	355.06	1.5
C6H13IO2	244.07	0.33
C6H10IN2O8	365.06	1.33
C6H10IO3	257.05	0.5
C6H6IN2O2	265.03	0.33
C6H8IO4	271.03	0.67
C6H13I2O	354.98	0.17
C7H12IN2O5	331.09	0.71
C7H10IO4	285.06	0.57
C7H16IO5	307.1	0.71
C7H9IO7	332.05	1
C7H8IO8	347.04	1.14
C7H8IO7	331.04	1
C7H14IO8	353.09	1.14
C7H6IN2O5	325.04	0.71
C7H14IO6	321.09	0.86
C7H8IO6	315.04	0.86
C7H12IN2O4	315.09	0.57
C7H16IO8	355.1	1.14
C7H11INO5	316.07	0.71
C7H7O7	203.13	1
C7H10IO6	317.06	0.86
C7H12IO6	319.07	0.86

C7H15I2O2	385	0.29
C7H11INO6	332.07	0.86
C7H14IO3	273.09	0.43
C7H8IO4	283.04	0.57
C7H8IO5	299.04	0.71
C7H16IO9	371.1	1.29
C7H11IO6	318.06	0.86
C7H12IO7	335.07	1
C7H14IO5	305.09	0.71
C7H10IO3	269.06	0.43
C7H14IN2O7	365.1	1
C7H12IO4	287.07	0.57
C7H14IO7	337.09	1
C7H12IO3	271.07	0.43
C7H10IO5	301.06	0.71
C7H11IO7	334.06	1
C7H11IO5	302.06	0.71
C7H12IO5	303.07	0.71
C7H13IO5	304.08	0.71
C7H6IN2O	261.04	0.14
C7H10IO7	333.05	1
C8H16IO5	319.11	0.63
C8H10IO8	361.06	1
C8H16IO8	367.11	1
C8H10IN2O6	357.08	0.75
C8H10INO6	343.07	0.75
C8H12IO8	363.08	1
C8H18IO7	353.13	0.88
C8H15IO6	334.11	0.75
C8H16IN2O6	363.13	0.75
C8H10IO6	329.07	0.75
C8H10IO7	345.07	0.88
C8H12IO7	347.08	0.88
C8H12IO6	331.08	0.75
C8H14IO6	333.1	0.75
C8H16IO6	335.11	0.75
C8H13IO6	332.09	0.75
C8H12IN2O6	359.1	0.75
C8H14IO5	317.1	0.63
C8H11INO7	360.08	0.88
C8H11IO2	266.08	0.25

C8H3IO5	306.01	0.63
C8H12IO4	299.08	0.5
C8H17I2O2	399.03	0.25
C8H9IO	248.06	0.13
C8H12IO3	283.08	0.38
C8H14IO3	285.1	0.38
C8H16IO4	303.11	0.5
C8H16IO3	287.12	0.38
C8H10IN2O3	309.08	0.38
C8H14IO4	301.1	0.5
C8H9IO5	312.06	0.63
C8H11INO4	312.08	0.5
C8H18IO3	289.13	0.38
C8H11O6	203.17	0.75
C8H11O5	187.17	0.63
C8H10IO5	313.07	0.63
C8H13IO4	300.09	0.5
C8H16IN2O3	315.13	0.38
C8H15INO4	316.11	0.5
C8H10IO4	297.07	0.5
C8H15INO3	300.11	0.38
C9H20IO7	367.16	0.78
C9H12IO6	343.09	0.67
C9H10IO8	373.08	0.89
C9H12I2O2	406	0.22
C9H13INO9	406.11	1
C9H10IO2	277.08	0.22
C9H14IO6	345.11	0.67
C9H18IN2O4	345.15	0.44
C9H16IO6	347.12	0.67
C9H11O8	247.18	0.89
C9H11O7	231.18	0.78
C9H22IN2O9	429.18	1
C9H19I2O5	461.05	0.56
C9H24IO6	355.19	0.67
C9H14IO7	361.11	0.78
C9H15O5	203.21	0.56
C9H14IN2O5	357.12	0.56
C9H15INO6	360.12	0.67
C9H11IO7	358.08	0.78
C9H18IO7	365.14	0.78

C9H12IO8	375.09	0.89
C9H7IO4	306.05	0.44
C9H18IO4	317.14	0.44
C9H12IO4	311.09	0.44
C9H14IN2O3	325.12	0.33
C9H16IO5	331.12	0.56
C9H14IO3	297.11	0.33
C9H17IO5	332.13	0.56
C9H12IN2O3	323.11	0.33
C9H11IO5	326.09	0.56
C9H15INO3	312.12	0.33
C9H14IO4	313.11	0.44
C9H18IO3	301.14	0.33
C9H14IO8	377.11	0.89
C9H18IO9	397.14	1
C9H12IO5	327.09	0.56
C9H16IO3	299.13	0.33
C9H18IO5	333.14	0.56
C9H14IO5	329.11	0.56
C10H22IO8	397.18	0.8
C10H14IO8	389.12	0.8
C10H20IO8	395.17	0.8
C10H16IO8	391.13	0.8
C10H22IN2O4	361.2	0.4
C10H17IO6	360.14	0.6
C10H24IN2O6	395.21	0.6
C10H18IO6	361.15	0.6
C10H21I2O2	427.08	0.2
C10H15INO7	388.13	0.7
C10H18IO9	409.15	0.9
C10H20IO6	363.17	0.6
C10H17INO8	406.15	0.8
C10H12IO8	387.1	0.8
C10H14IN2O6	385.13	0.6
C10H10IO9	401.09	0.9
C10H13IO9	404.11	0.9
C10H15INO8	404.13	0.8
C10H18IO7	377.15	0.7
C10H15I2O	405.03	0.1
C10H24IO6	367.2	0.6
C10H12IO7	371.1	0.7

C10H14IO9	405.12	0.9
C10H14IO7	373.12	0.7
C10H24IO9	415.2	0.9
C10H16IO7	375.13	0.7
C10H6IO5	333.06	0.5
C10H12IO5	339.1	0.5
C10H18IO3	313.15	0.3
C10H14IN2O3	337.13	0.3
C10H10IO5	337.09	0.5
C10H15O7	247.22	0.7
C10H13O8	261.21	0.8
C10H20IO2	299.17	0.2
C10H10IO3	305.09	0.3
C10H11IO3	306.1	0.3
C10H16IN2O3	339.15	0.3
C10H14IO3	309.12	0.3
C10H18IO4	329.15	0.4
C10H18IN2O	309.17	0.1
C10H16IO4	327.14	0.4
C10H15IO4	326.13	0.4
C10H16IO3	311.14	0.3
C10H18IN2O2	325.17	0.2
C10H16IN2O2	323.15	0.2
C10H10IN2O2	317.1	0.2
C10H16IO6	359.13	0.6
C10H13IO5	340.11	0.5
C10H19N2O9	311.27	0.9
C10H10IN2O4	349.1	0.4
C10H18IN2O4	357.17	0.4
C10H15O6	231.22	0.6
C10H15INO4	340.13	0.4
C10H20IO5	347.17	0.5
C10H19O4	203.26	0.4
C10H15IO5	342.13	0.5
C10H14IO5	341.12	0.5
C10H16IO5	343.14	0.5
C10H16O6	232.23	0.6
C10H15IO6	358.13	0.6
C11H18IO6	373.16	0.55
C11H16IO7	387.15	0.64
C11H20IO3	327.18	0.27

C11H26IO8	413.22	0.73
C11H24IO8	411.21	0.73
C11H22IO3	329.2	0.27
C11H14IO8	401.13	0.73
C11H22IO9	425.19	0.82
C11H24IN2O7	423.22	0.64
C11H14IO6	369.13	0.55
C11H18IO9	421.16	0.82
C11H19IO4	342.17	0.36
C11H20O5	232.27	0.45
C12H16IO11	463.15	0.92
C12H16O4	224.25	0.33
C12H16IO8	415.16	0.67
C12H16IO7	399.16	0.58
C12H20IN2O5	399.2	0.42
C12H16IN2O7	427.17	0.58
C12H25INO6	406.23	0.5
C12H15INO8	428.15	0.67
C12H24IO4	359.22	0.33
C12H18IO7	401.17	0.58
C12H18IO5	369.17	0.42
C12H19O12	355.27	1
C12H17IO4	352.17	0.33
C12H15IO3	334.15	0.25
C12H20IO5	371.19	0.42
C12H16IO6	383.16	0.5
C13H28IN2O2	371.28	0.15
C13H24IO4	371.23	0.31
C13H18IO7	413.18	0.54
C13H22IO4	369.22	0.31
C13H18IO5	381.18	0.38
C13H20IO7	415.2	0.54
C13H16IO7	411.17	0.54
C13H20IO5	383.2	0.38
C13H22IN2O4	397.23	0.31
C13H14IO3	345.15	0.23
C13H22IO3	353.22	0.23
C13H19INO7	428.2	0.54
C13H18IO8	429.18	0.62
C14H15INO6	420.18	0.43
C14H22IO3	365.23	0.21

C14H16IO7	423.18	0.5
C14H22IO6	413.23	0.43
C14H20IO6	411.21	0.43
C14H18IO9	457.19	0.64
C14H20IO8	443.21	0.57
C14H16IO6	407.18	0.43
C14H15IO4	374.17	0.29
C14H22IO4	381.23	0.29
C14H26IO4	385.26	0.29
C14H22IN2O4	409.24	0.29
C14H28IO2	355.28	0.14
C14H23I2O	461.14	0.07
C15H22IO7	441.24	0.47
C15H26IO6	429.27	0.4
C15H18IO4	389.21	0.27
C15H16IO2	355.19	0.13
C15H24IO6	427.25	0.4
C15H20IO	343.22	0.07
C15H30IN2O2	397.32	0.13
C15H30IO4	401.3	0.27
C15H22IO3	377.24	0.2
C16H32IO2	383.33	0.13
C16H28IO4	411.3	0.25
C16H17INO5	430.21	0.31
C16H22IO7	453.25	0.44
C16H26IO6	441.28	0.38
C16H26IO7	457.28	0.44
C16H31INO4	428.33	0.25
C16H20IO3	387.23	0.19
C16H21O4	277.34	0.25
C16H28IO5	427.3	0.31
C16H19IO4	402.22	0.25
C16H22IO	357.25	0.06
C16H18IO3	385.22	0.19
C17H28IO7	471.3	0.41
C17H26IO6	453.29	0.35
C17H28IO6	455.31	0.35
C17H26IO4	421.29	0.24
C17H22IO3	401.26	0.18
C18H24IN2O3	443.3	0.17
C18H38IO3	429.4	0.17

C18H20IO4	427.25	0.22
C18H34IO3	425.37	0.17
C18H36IO2	411.38	0.11
C18H19INO6	472.25	0.33
C18H21INO5	458.27	0.28
C18H22IO6	461.27	0.33
C18H25N2O8	397.4	0.44
C18H34IO4	441.36	0.22
C18H21INO6	474.27	0.33
C19H20IO5	455.26	0.26
C19H20IO6	471.26	0.32
C20H19N2O7	399.37	0.35
C20H15O9	399.33	0.45

6.2 Arial drone images for each day of the clearcut



Figure S1: Drone images for each day of the clearcut (2022-07-24 to 2022-07-29).

6.3 Signal variation with carbon and oxygen

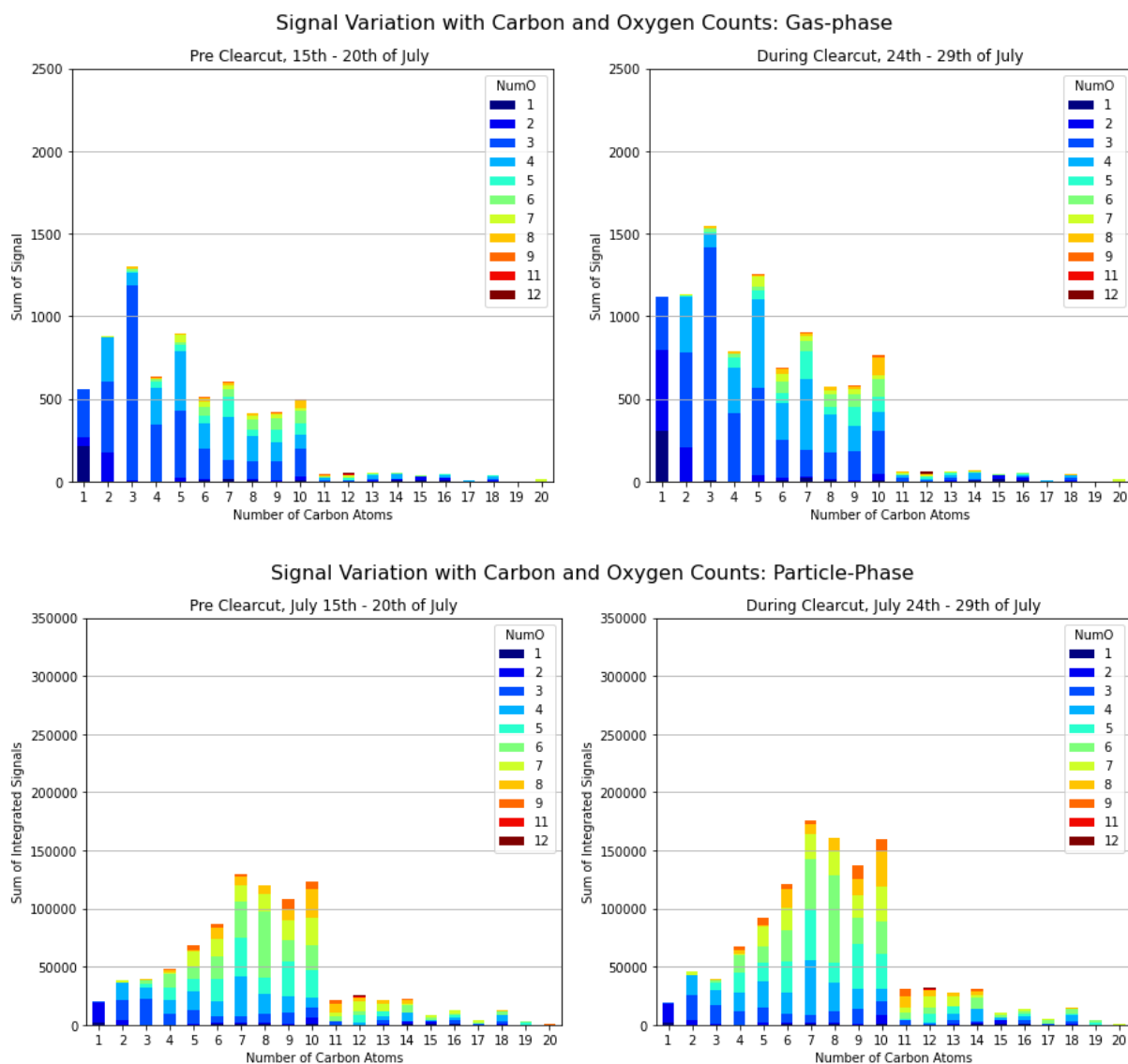


Figure S2: Number of different types of compounds during pre-clearcut and active-clearcut period in gas- and particle-phase. The y-axis shows the sum of signals for compounds that have the same number of carbons. The x-axis shows number of carbons for each bar the is plotted. The colour shows how many oxygens compounds with the same number of carbons had.

7 References

- Ahlström, A., Canadell, J. G., & Metcalfe, D. B. (2022). Widespread Unquantified Conversion of Old Boreal Forests to Plantations. *Earth's future*, *10*(11), n/a. <https://doi.org/10.1029/2022EF003221>
- Barreira, L. M. F., Ylisirnio, A., Pullinen, I., Buchholz, A., Li, Z., Lipp, H., Junninen, H., Horrak, U., Noe, S. M., Krasnova, A., Krasnov, D., Kask, K., Talts, E., Niinemets, U., Ruiz-Jimenez, J., & Schobesberger, S. (2021). The importance of sesquiterpene oxidation products for secondary organic aerosol formation in a springtime hemiboreal forest. *Atmospheric chemistry and physics*, *21*(15), 11781-11800. <https://doi.org/10.5194/acp-21-11781-2021>
- Bergström, R., Hallquist, M., Simpson, D., Wildt, J., & Mentel, T. F. (2014). Biotic stress: a significant contributor to organic aerosol in Europe? *Atmos. Chem. Phys.*, *14*(24), 13643-13660. <https://doi.org/10.5194/acp-14-13643-2014>
- Bertram, T. H., Kimmel, J. R., Crisp, T. A., Ryder, O. S., Yatavelli, R. L. N., Thornton, J. A., Cubison, M. J., Gonin, M., & Worsnop, D. R. (2011). A field-deployable, chemical ionization time-of-flight mass spectrometer. *Atmospheric measurement techniques*, *4*(7), 1471-1479. <https://doi.org/10.5194/amt-4-1471-2011>
- Chan, M. N., Surratt, J. D., Chan, A. W. H., Schilling, K., Offenberg, J. H., Lewandowski, M., Edney, E. O., Kleindienst, T. E., Jaoui, M., Edgerton, E. S., Tanner, R. L., Shaw, S. L., Zheng, M., Knipping, E. M., & Seinfeld, J. H. (2011). Influence of aerosol acidity on the chemical composition of secondary organic aerosol from β -caryophyllene. *Atmospheric chemistry and physics*, *11*(4), 1735-1751. <https://doi.org/10.5194/acp-11-1735-2011>
- D'Ambro, E. L., Lee, B. H., Liu, J., Shilling, J. E., Gaston, C. J., Lopez-Hilfiker, F. D., Schobesberger, S., Zaveri, R. A., Mohr, C., Lutz, A., Zhang, Z., Gold, A., Surratt, J. D., Rivera-Rios, J. C., Keutsch, F. N., & Thornton, J. A. (2017). Molecular composition and volatility of isoprene photochemical oxidation secondary organic aerosol under low- and high-NO_x conditions. *Atmospheric chemistry and physics*, *17*(1), 159-174. <https://doi.org/10.5194/acp-17-159-2017>
- D'Ambro, E. L., Hyttinen, N., Møller, K. H., Iyer, S., Otkjær, R. V., Bell, D. M., Liu, J., Lopez-Hilfiker, F. D., Schobesberger, S., Shilling, J. E., Zelenyuk, A., Kjaergaard, H. G., Thornton, J. A., & Kurtén, T. (2022). Pathways to Highly Oxidized Products in the Δ^3 -Carene + OH System. *Environmental science & technology*, *56*(4).
- Dbouk, Z., Belhadj, N., Lailliau, M., Benoit, R., & Dagaut, P. (2024). On the autoxidation of terpenes: Detection of oxygenated and aromatic products. *Fuel (Guildford)*, *358*(Part B), 130306. <https://doi.org/10.1016/j.fuel.2023.130306>
- Finlayson-Pitts, B. J. (2000). *Chemistry of the upper and lower atmosphere theory, experiments, and applications*. San Diego : Academic Press.
- Fujimura, C. (2023). *Impacts of boreal forest management (clear-cut) on volatile organic compound emissions and their oxidation products* [Stockholm University].

- Ghirardo, A., Koch, K., Taipale, R., Zimmer, I. N. A., Schnitzler, J.-P., & Rinne, J. (2010). Determination of de novo and pool emissions of terpenes from four common boreal/alpine trees by $^{13}\text{CO}_2$ labelling and PTR-MS analysis. *Plant, cell and environment*, 33(5), 781-792. <https://doi.org/10.1111/j.1365-3040.2009.02104.x>
- Goldstein, A. H., & Galbally, I. E. (2007). Known and Unexplored Organic Constituents in the Earth's Atmosphere. *Environmental science & technology*, 41(5), 1514-1521. <https://doi.org/10.1021/es072476p>
- Haapanala, S., Hakola, H., Hellén, H., Vestenius, M., Levula, J., & Rinne, J. (2012). Is forest management a significant source of monoterpenes into the boreal atmosphere? *Biogeosciences*, 9(4), 1291-1300. <https://doi.org/10.5194/bg-9-1291-2012>
- Hallquist, M., Wenger, J. C., Baltensperger, U., Rudich, Y., Simpson, D., Claeys, M., Dommen, J., Donahue, N. M., George, C., Goldstein, A. H., Hamilton, J. F., Herrmann, H., Hoffmann, T., Iinuma, Y., Jang, M., Jenkin, M. E., Jimenez, J. L., Kiendler-Scharr, A., Maenhaut, W., McFiggans, G., Mentel, T. F., Monod, A., Prévôt, A. S. H., Seinfeld, J. H., Surratt, J. D., Szmigielski, R., & Wildt, J. (2009). The formation, properties and impact of secondary organic aerosol: Current and emerging issues. *Atmospheric chemistry and physics*, 9(14), 5155-5236. <https://doi.org/10.5194/acp-9-5155-2009>
- Hamilton, J. F., Rami Alfarra, M., Wyche, K. P., Ward, M. W., Lewis, A. C., McFiggans, G. B., Good, N., Monks, P. S., Carr, T., White, I. R., & Purvis, R. M. (2011). Investigating the use of secondary organic aerosol as seed particles in simulation chamber experiments. *Atmospheric chemistry and physics*, 11(12), 5917-5929. <https://doi.org/10.5194/acp-11-5917-2011>
- Hammes, J., Lutz, A., Mentel, T., Faxon, C., & Hallquist, M. (2019). Carboxylic acids from limonene oxidation by ozone and hydroxyl radicals: insights into mechanisms derived using a FIGAERO-CIMS. *Atmospheric chemistry and physics*, 19(20), 13037-13052. <https://doi.org/10.5194/acp-19-13037-2019>
- Han, S., & Jang, M. (2023). Modeling daytime and nighttime secondary organic aerosol formation via multiphase reactions of biogenic hydrocarbons. *Atmospheric chemistry and physics*, 23(2), 1209-1226. <https://doi.org/10.5194/acp-23-1209-2023>
- Hertog, I. M., Brogaard, S., & Krause, T. (2022). Barriers to expanding continuous cover forestry in Sweden for delivering multiple ecosystem services. *Ecosystem services*, 53, 101392. <https://doi.org/10.1016/j.ecoser.2021.101392>
- Hüve, K., Bichele, I., Rasulov, B., & Niinemets, Ü. (2011). When it is too hot for photosynthesis: heat-induced instability of photosynthesis in relation to respiratory burst, cell permeability changes and H_2O_2 formation. *Plant, cell and environment*, 34(1), 113-126. <https://doi.org/10.1111/j.1365-3040.2010.02229.x>

- Jenkin, M. E., Saunders, S. M. and Pilling, M. J.: The tropospheric degradation of volatile organic compounds: A protocol for mechanism development, *Atmos. Environ.*, 31(1), 81–104, doi:10.1016/S1352-2310(96)00105-7, 1997. Jenkin, M. E., Young, J. C. and Rickard, A. R.: The MCM v3.3.1 degradation scheme for isoprene, *Atmos. Chem. Phys.*, 15(20), 11433–11459, doi:10.5194/acp-15-11433-2015, 2015.
- Kivimäenpää, M., Magsarjav, N., Ghimire, R., Markkanen, J.-M., Heijari, J., Vuorinen, M., & Holopainen, J. K. (2012). Influence of tree provenance on biogenic VOC emissions of Scots pine (*Pinus sylvestris*) stumps. *Atmospheric environment (1994)*, 46, 477-485. <https://doi.org/10.1016/j.atmosenv.2012.07.018>
- Krechmer, J., Lopez-Hilfiker, F., Koss, A., Hutterli, M., Stoerner, C., Deming, B., Kimmel, J., Warneke, C., Holzinger, R., Jayne, J., Worsnop, D., Fuhrer, K., Gonin, M., & de Gouw, J. (2018). Evaluation of a New Reagent-Ion Source and Focusing Ion–Molecule Reactor for Use in Proton-Transfer-Reaction Mass Spectrometry. *Analytical chemistry (Washington)*, 90(20), 12011-12018. <https://doi.org/10.1021/acs.analchem.8b02641>
- Kristensen, K., Cui, T., Zhang, H., Gold, A., Glasius, M., & Surratt, J. D. (2014). Dimers in α -pinene secondary organic aerosol: effect of hydroxyl radical, ozone, relative humidity and aerosol acidity. *Atmospheric chemistry and physics*, 14(8), 4201-4218. <https://doi.org/10.5194/acp-14-4201-2014>
- Kundu, S., Fisseha, R., Putman, A. L., Rahn, T. A., & Mazzoleni, L. R. (2017). Molecular formula composition of β -caryophyllene ozonolysis SOA formed in humid and dry conditions. *Atmospheric environment (1994)*, 154(C), 70-81. <https://doi.org/10.1016/j.atmosenv.2016.12.031>
- Lee, B. H., Lopez-Hilfiker, F. D., Mohr, C., Kurtén, T., Worsnop, D. R., & Thornton, J. A. (2014). An Iodide-Adduct High-Resolution Time-of-Flight Chemical-Ionization Mass Spectrometer: Application to Atmospheric Inorganic and Organic Compounds. *Environmental science & technology*, 48(11), 6309-6317. <https://doi.org/10.1021/es500362a>
- Lindahl, K. B., Sténs, A., Sandström, C., Johansson, J., Lidskog, R., Ranius, T., & Roberge, J.-M. (2017). The Swedish forestry model: More of everything? *Forest policy and economics*, 77, 44-55. <https://doi.org/10.1016/j.forpol.2015.10.012>
- Litvak, M., & Monson, R. (1998). Patterns of Induced and Constitutive Monoterpene Production in Conifer Needles in Relation to Insect Herbivory. *Oecologia*, 114(4), 531-540. <https://doi.org/10.1007/s004420050477>
- Liu, D., Zhang, Y., Zhong, S., Chen, S., Xie, Q., Zhang, D., Zhang, Q., Hu, W., Deng, J., Wu, L., Ma, C., Tong, H., & Fu, P. (2023). Large differences of highly oxygenated organic molecules (HOMs) and low-volatile species in secondary organic aerosols (SOAs) formed from ozonolysis of β -pinene and limonene. *Atmospheric chemistry and physics*, 23(14), 8383-8402. <https://doi.org/10.5194/acp-23-8383-2023>

- Liu, X., Deming, B., Pagonis, D., Day, D. A., Palm, B. B., Talukdar, R., Roberts, J. M., Veres, P. R., Krechmer, J. E., Thornton, J. A., de Gouw, J. A., Ziemann, P. J., & Jimenez, J. L. (2019). Effects of gas-wall interactions on measurements of semivolatile compounds and small polar molecules. *Atmospheric measurement techniques*, *12*(6), 3137-3149. <https://doi.org/10.5194/amt-12-3137-2019>
- Liu, Y., Kuwata, M., McKinney, K. A., & Martin, S. T. (2016). Uptake and release of gaseous species accompanying the reactions of isoprene photo-oxidation products with sulfate particles. *Physical chemistry chemical physics : PCCP*, *18*(3), 1595-1600. <https://doi.org/10.1039/c5cp04551g>
- Liu, Y., Wang, H., Jing, S., Gao, Y., Peng, Y., Lou, S., Cheng, T., Tao, S., Li, L., Li, Y., Huang, D., Wang, Q., & An, J. (2019). Characteristics and sources of volatile organic compounds (VOCs) in Shanghai during summer: Implications of regional transport. *Atmospheric environment (1994)*, *215*, 116902. <https://doi.org/10.1016/j.atmosenv.2019.116902>
- Lopez-Hilfiker, F. D., Mohr, C., Ehn, M., Rubach, F., Kleist, E., Wildt, J., Mentel, T. F., Lutz, A., Hallquist, M., Worsnop, D., & Thornton, J. A. (2014). A novel method for online analysis of gas and particle composition: description and evaluation of a Filter Inlet for Gases and AEROSols (FIGAERO). *Atmospheric Measurement Techniques*, *2014*, Vol. 7, Iss. 4, pp. 983-1001, *7*(4), 983-1001.
- Loreto, F., & Schnitzler, J.-P. (2010). Abiotic stresses and induced BVOCs: Induced biogenic volatile organic compounds from plants. *Trends in plant science*, *15*(3), 154-166.
- Masoud, C. G., Li, Y., Wang, D. S., Katz, E. F., DeCarlo, P. F., Farmer, D. K., Vance, M. E., Shiraiwa, M., & Hildebrandt Ruiz, L. (2022). Molecular composition and gas-particle partitioning of indoor cooking aerosol: Insights from a FIGAERO-CIMS and kinetic aerosol modeling. *Aerosol science and technology*, *56*(12), 1156-1173. <https://doi.org/10.1080/02786826.2022.2133593>
- Mäki, M., Aalto, J., Hellén, H., Pihlatie, M., & Bäck, J. (2019). Interannual and seasonal dynamics of volatile organic compound fluxes from the boreal forest floor. *Frontiers in plant science*, *10*, 191-191. <https://doi.org/10.3389/fpls.2019.00191>
- Nelson, B. S., Stewart, G. J., Drysdale, W. S., Newland, M. J., Vaughan, A. R., Dunmore, R. E., Edwards, P. M., Lewis, A. C., Hamilton, J. F., Acton, W. J., Hewitt, C. N., Crilley, L. R., Alam, M. S., Şahin, Ü. A., Beddows, D. C. S., Bloss, W. J., Slater, E., Whalley, L. K., Heard, D. E., Cash, J. M., Langford, B., Nemitz, E., Sommariva, R., Cox, S., Shivani, Gadi, R., Gurjar, B. R., Hopkins, J. R., Rickard, A. R., and Lee, J. D.: In situ ozone production is highly sensitive to volatile organic compounds in Delhi, India, *Atmos. Chem. Phys.*, *21*, 13609–13630, <https://doi.org/10.5194/acp-21-13609-2021>, 2021.
- Raisanen, T., Ryyppo, A., & Kellomaki, S. (2009). Monoterpene emission of a boreal Scots pine (*Pinus sylvestris* L.) forest. *Agricultural and forest meteorology*, *149*(5), 808-819. <https://doi.org/10.1016/j.agrformet.2008.11.001>

- Rinne, J., Markkanen, T., Ruuskanen, T. M., Petäjä, T., Keronen, P., Tang, M. J., Crowley, J. N., Rannik, Ä., & Vesala, T. (2012). Effect of chemical degradation on fluxes of reactive compounds – a study with a stochastic Lagrangian transport model. *Atmospheric chemistry and physics*, *12*(11), 4843-4854. <https://doi.org/10.5194/acp-12-4843-2012>
- Sato, E., Matsumoto, K., Okochi, H., & Igawa, M. (2006). Scavenging Effect of Precipitation on Volatile Organic Compounds in Ambient Atmosphere. *Bulletin of the Chemical Society of Japan*, *79*(8), 1231-1233. <https://doi.org/10.1246/bcsj.79.1231>
- Seinfeld, J. H. (2016). *Atmospheric Chemistry and Physics : From Air Pollution to Climate Change* (3. uppl. ed.). John Wiley & Sons.
- Skogsstyrelsen. (2022). *Bruttoavverkning 2020 med preliminär statistik för 2021 och prognos för 2022*. <https://www.skogsstyrelsen.se/statistik/statistik-efter-amne/avverkning/>
- Vanhatalo, A., Chan, T., Aalto, J., Korhonen, J. F., Kolari, P., Hölttä, T., Nikinmaa, E., & Bäck, J. (2015). Tree water relations can trigger monoterpene emissions from Scots pine stems during spring recovery. *Biogeosciences*, *12*(18), 5353-5363. <https://doi.org/10.5194/bg-12-5353-2015>
- Vestenius, M., Hopke, P. K., Lehtipalo, K., Petäjä, T., Hakola, H., & Hellén, H. (2021). Assessing volatile organic compound sources in a boreal forest using positive matrix factorization (PMF). *Atmospheric environment (1994)*, *259*, 118503. <https://doi.org/10.1016/j.atmosenv.2021.118503>
- Wang, D., Masoud, C., Modi, M., & Ruiz, L. (2022, 06/14). Isoprene–Chlorine Oxidation in the Presence of NO_x and Implications for Urban Atmospheric Chemistry. *Environmental science & technology*, *56*. <https://doi.org/10.1021/acs.est.1c07048>
- Wang, H., Ma, X., Tan, Z., Wang, H., Chen, X., Chen, S., Gao, Y., Liu, Y., Liu, Y., Yang, X., Yuan, B., Zeng, L., Huang, C., Lu, K., & Zhang, Y. (2022). Anthropogenic monoterpenes aggravating ozone pollution. *National science review*, *9*(9), nwac103-nwac103. <https://doi.org/10.1093/nsr/nwac103>
- Wang, X., Zhang, Y., Tan, Y., Tan, Y., Bai, J., Gu, D., Ma, Z., Du, J., & Han, Z. (2022). Effects of light on the emissions of biogenic isoprene and monoterpenes: A review. *Atmospheric pollution research*, *13*(5), 101397. <https://doi.org/10.1016/j.apr.2022.101397>
- Yee, L. D., Isaacman-VanWertz, G., Wernis, R. A., Meng, M., Rivera, V., Kreisberg, N. M., Hering, S. V., Bering, M. S., Glasius, M., Upshur, M. A., Bé, A. G., Thomson, R. J., Geiger, F. M., Offenberg, J. H., Lewandowski, M., Kourtchev, I., Kalberer, M., de Sá, S., Martin, S. T., Alexander, M. L., Palm, B. B., Hu, W., Campuzano-Jost, P., Day, D. A., Jimenez, J. L., Liu, Y., McKinney, K. A., Artaxo, P., Viegas, J., Manzi, A., Oliveira, M. B., de Souza, R., Machado, L. A. T., Longo, K., & Goldstein, A. H. (2018). Observations of sesquiterpenes and their oxidation products in central Amazonia during the wet and dry seasons. *Atmospheric chemistry and physics*, *18*(14), 10433-10457. <https://doi.org/10.5194/acp-18-10433-2018>

Zhang, H., Yee, L. D., Lee, B. H., Curtis, M. P., Worton, D. R., Isaacman-VanWertz, G., Offenberg, J. H., Lewandowski, M., Kleindienst, T. E., Beaver, M. R., Holder, A. L., Lonneman, W. A., Docherty, K. S., Jaoui, M., Pye, H. O. T., Hu, W., Day, D. A., Campuzano-Jost, P., Jimenez, J. L., Guo, H., Weber, R. J., De Gouw, J., Koss, A. R., Edgerton, E. S., Brune, W., Mohr, C., Lopez-Hilfiker, F. D., Lutz, A., Kreisberg, N. M., Spielman, S. R., Hering, S. V., Wilson, K. R., Thornton, J. A., & Goldstein, A. H. (2018). Monoterpenes are the largest source of summertime organic aerosol in the southeastern United States. *Proceedings Of The National Academy Of Sciences Of The United States Of America*, 2018, Vol. 115, Iss. 9, pp. 2038-2043, 115(9), 2038-2043.